JIMMA UNIVERSITY

JIMMA INSTITUTE OF TECHNOLOGY

FACULTY OF MECHANICAL ENGINEERING

FATIGUE ANALYSIS OF STEAM TURBINE BLADE (STB)

CASE STUDY: FINCHAA SUGAR FACTORY

A thesis submitted to the school of graduate studies of Jimma University, Jimma Institute of Technology in partial fulfillment for the requirement of the Degree of Masters of Science in Mechanical Engineering (Design of Mechanical Systems Stream)

By: Mr. Moti Tekalign Feyisa

June 18, 2021

Jimma-Ethiopia

JIMMA UNIVERSITY

JIMMA INSTITUTE OF TECHNOLOGY

FACULTY OF MECHANICAL ENGINEERING

FATIGUE ANALYSIS OF STEAM TURBINE BLADE (STB)

CASE STUDY: FINCHAA SUGAR FACTORY

A thesis submitted to the school of graduate studies of Jimma University, Jimma Institute of Technology in partial fulfillment for the requirement of the Degree of Masters of Science in Mechanical Engineering (Design of Mechanical Systems Stream)

By: Mr. Moti Tekalign Feyisa

Advisor: Dr.-Ing. Getachew Shunki Tibba

Co-advisor: Dr. Johnson Santhosh

June 18, 2021

Jimma-Ethiopia

DECLARATION

I hereby declare that this submission is my own work and that, to the best of my knowledge and belief, it contains no material previously published or written by another person for the award of any other degree or diploma of the university or other institute of higher learning which is entitled **" Fatigue Analysis of Steam Turbine Blade: Case Study on Finchaa Sugar Factory"** except where due acknowledgment has been made in the text. Any scholarly matter that is included in the thesis has been given recognition through citation.

Mr.Moti Tekalign _____ _____

Candidate Signature Date

APPROVAL SHEET

As a member of the Examination Board of the final Master of Science open defense, we certify that we have read and evaluated the thesis prepared by Mr.Moti Tekalign Feyisa entitled **"Fatigue Analysis of Steam Turbine Blade: Case Study on Finchaa Sugar Factory"**. We recommend that it could be accepted as a fulfilling the thesis requirement for the Degree of Master of Science in Mechanical Engineering (Design of Mechanical System).

Dr-Ing. Getachew Shunki	_____	_____
Main-Advisor	Signature	Date
Dr. Johonson Santosh	_____	_____
Co-advisor	Signature	Date
Mr. Iyasu Tafese	_____	_____
Chairperson	Signature	Date

Examination members

1. Dr. Moera Gutu	_____	_____
External examiner	Signature	Date
2. Dr-Ing. Mesay Alemu	_____	_____-
Internal examiner	Signature	Date

THESIS CERTIFICATE

This is to certify that the thesis entitled **"Fatigue Analysis of Steam Turbine Blade: Case Study on Finchaa Sugar Factory"** submitted by Mr. Moti Tekalign Feyisa to Jimma Institute of Technology towards partial fulfillment of the requirements for the award of the degree of Master of Technology in Mechanical Engineering (Design of Mechanical System) is a bona fide record of the work carried out by him under my supervision and guidance.

Dr.Ing. Getachew Shunki _____ _____

Main-Advisor Signature Date

Department of Mechanical Engineering

Addis Ababa Science and Technology University(AASTU)

Addis Ababa, Ethiopia.

Dr. Johonson Santosh _____- _____

Co-advisor Signature Date

Department of Mechanical Engineering

Jimma University, Jimma Institute of Technology(JiT)

Jimma, Ethiopia.

Dedicated To

My

Beloved Family

ABSTRACT

The steam turbine handles the maximum power demand among all stationary prime movers that are used for electric power generation. A steam turbine is a constant volume machine. There are two basic types of steam turbines. The impulse stage is best suited for high-pressure region and for small steam quantities. The reaction stage is advantageous at the lower pressure region, where a large volume of steam must be handled. Both type of steam turbine is used in Finchaa Sugar Factory in four units; two impulses and two reactions. This study is focused on impulse steam turbine blade because it works for a twenty-one years ago. The main failure of steam turbine blade is due to corrosion fatigue failure, fritting fatigue failure and thermal fatigue failure. The main problem occurred on steam turbine blade in Finchaa Sugar Factory is due to thermal load which is depend on thermal properties of steam. The aim of this study is to predict the life of steam turbine blade through analysis of its thermal fatigue using computational fluid dynamics software packages. In Fluid-Structure Interaction method of analysis, both transient computational fluid dynamics and structural dynamics are mathematically modeled. To analyze the approximate solutions for transient state for both fluid and solid fourth ordered Runge Kutta initial value problem method is derived. The blade was then analyzed for the temperature and pressure distribution. After containing thermal load distribution, the blade was then analyzed for static structure. Results shows that the maximum total deformation is 5.755 mm and the maximum equivalent stress is 1983.8 MPa. Generally, steam turbine blade with given typical parameter here is operating for minimum of 19.42 years. This predicted fatigue life is due to the cause of thermal fatigue only.

Key Words: *Steam Turbine Blade, Fluid-Structure Interaction, fatigue life.*

ACKNOWLEDGMENT

Before anything, glory and thanks be to God who gives me full health, peace, knowledge and wisdom to accomplish this thesis work and he is still in my side throughout my life.

My deepest feeling of gratitude goes to my advisor Dr.Ing. Getachew Shunki (Ph.D. of Mechanical Engineering at Addis Ababa Science and Technology University), for his great advice, and constant encouragement helped me to complete this research work successfully. I never ever forget his admirable patience, work quality, and attractive spirit of friendship as unique personal possessions.

I would like to express my greatest gratitude and respect to my co-advisor Dr. Johnson Santhosh (Mechanical Engineering at JiT) for his excellent guidance, valuable suggestions and endless support.

I am thankful to Fincha Sugar Factory executive manager Mr. Silashi Dugasa for allowing me to take a data from steam power plant in the factory and I would like to thank Mr. Midagsa Buli for his support, appreciation and elderly advice. He is a chief mechanic on steam turbine in Fincha Sugar Factory for eight years ago.

Finally yet importantly, I would like to express my deepest gratitude to my families and my friends who stand beside me to complete my work.

Table of Contents

List of Figures

List of Tables

ACRONYMS AND ABBREVIATIONS

Acronyms/Abbreviation	Definition
CFD	Computational Fluid Dynamics
CAD	Computer Aided Design
FDM	Finite Difference Method
FEA	Finite Element Analysis
FEM	Finite Element Method
FVM	Finite Volume Method
FSI	Fluid Structure Interaction
GTP	Growth and Transformation Plan
HPT	High Pressure Turbine
IPT	Intermediate Pressure Turbine
LEFM	Linear Elastic Fracture Mechanics
LPT	Low Pressure Turbine
S-N	Mean Stress Verses Number of Cycle
SEM	Scanning Electron Microscope
STB	Steam Turbine Blade
NACA	National Advisory Committee for Aeronautics
AISI	American Iron and Steel Institute
e-N	Strain Verses Number of Cycle
3D	Three Dimensional

SYMBOLS

Symbols	Definition
f_x, f_y, f_z	Body force along x,y and z respectively
α	Coefficient of thermal expansion
ρ	Density of steam
$\sigma_x, \sigma_y, \sigma_z$	Distance along x,y and z respectively
N_f	Fatigue life (Number of cycle to failure)
$\sigma_f^{'}$	Fatigue Strength coefficient
b	Fatigue strength exponent
q	Heat flux vector
m	Mass flow rate of steam
N_i	Number of cycle for crack initiation
N_f	Number of cycle for crack propagation
v	Poison ratio
P	Pressure of steam
τ	Shear stresses on the steam
ε	Strain
ε_σ	Strain due to stress
ε_T	Strain due to temperature
$\mathbb{T}$	Stress deviator tensor
σ	Stress tensor
T	Temperature of steam
u, v, w	Velocity component of steam along x,y and z respectively
$\overrightarrow{V}$	Velocity Vector
E	Youngs modulus of AISI 420 stainless steel

σ_m	Mean stress
σ_a	Stress amplitude
σ_e	Endurance fatigue limit
σ_u	Ultimate tensile strength
σ_{VM}	Von Mises stress
σ_{max}	Maximum stress in fatigue load cycle
σ_{min}	Minimum stress in fatigue load cycle

Chapter 1

INTRODUCTION

1.1 Historical Perspective of Finchaa Sugar Factory

Fincha Sugar Factory is found in Oromia Regional State in Horro Guduru Wollega Zone, Abay Chomen district in Finchaa Rift Valley around 350 Kilometers away from the capital city of Ethiopia, Addis Ababa. Bukers Agricultural International Ltd. of Britain conducted feasibility study including the topography and soil content of the area since 1978, while the project work had started in 1989. The factory started production in 1998 and until 2018; the average annual production capacity of Fincha Sugar Factory was 110,000 tons of sugar while it had the capacity of producing 8,000-meter cube ethanol. Figure 1.1a) shows that the location of Finchaa Sugar Factory on map and b)shows the front view of Finchaa Sugar Factory.

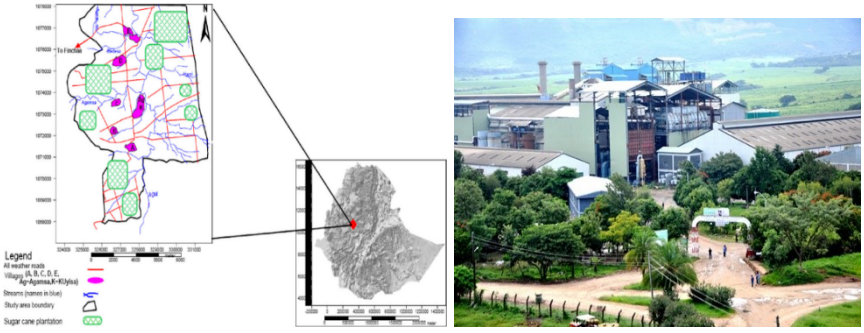

Figure 1.1: a) Map of Finchaa Sugar Factory b) View of Finchaa Sugar Factory

In Finchaa Sugar Factory, there are different plants: cane preparation plant, cane milling and juice extraction plant, clarification plant, boiler plant, ethanol production plant and electric power generation plant. In electric power generation plant turbine and generator is the main machine to be used. Since the prime mover for the turbine is pressurized steam, which is generated in boiler plant. This steam is supplied continuously to form rotation of the turbine, which is connected to generator shaft to generate electricity. Steam turbine used in Finchaa

Sugar Factory is a single stage impulse turbine. The operating speed of this turbine is 5970 rpm at normal condition. The serial number of this steam turbine is D-3943.

1.2 Background of the Study

In Ethiopia, the expansion of different industry is ongoing after growth and transformation plan (GTP). Those industries are like textile industry, agro-economic industry, tannery industry, sugar industry, metal industry, etc. Sugar Factory is one of the oldest and popular industry in the country for further establishment and expansion. From more than ten of sugar factories in Ethiopia, Fincha Sugar Factory is the oldest in production of sugar and ethanol. Most of industries in Ethiopia use electric power for their production. This electric power is supplied from national grid. However, in some sugar factories the electric power consumed is generated from synchronized system of boiler plant, steam turbine and generator inside the factory. A steam turbine is a device that extracts thermal energy from pressurized steam and uses it to do mechanical work on a rotating output shaft which is connected to the rotor of generator [1, 2]. The steam is generated in boiler plant from purified water, using by-product of sugar cane (bagasse) as a fuel. From steam turbine components, rotating blade is the most common and very essential part. There are two basic types of turbine blade, reaction turbine blade and impulse turbine blade [3]. Impulse type of turbine blade is used in Finchaa Sugar Factory (FSF). Since steam is applied on the blade cyclically for a long period, different fatigue failure is occurring at different pressure stages of steam turbine. Corrosion failure, fretting fatigue failure and Thermal fatigue failures are the most common failure that affects life of the blade [4]. In the low-pressure stage of steam turbine corrosion failure is occurring due to pressure and temperature drop. Steam turbine blade is corroding when a chemical reaction is taking place in between the blade material and wet steam [5]. At corrode part of the blade scratching, pitting and holes is the area at which stress concentration is very high which leads to crack nucleation and initiation. Formation of corrosion pits on the blade airfoil region results in distortion of steam passages, which in turn alters steam velocities and pressure drops, which can cause excessive rotor thrust causing vibration problems. After a period, crack is growing and the turbine blade is failed [6, 7]. Fritting fatigue failure occurs in all components of the turbine due to centrifugal force and vibration of the components. Thermal fatigue failure occurs in high-pressure stage of steam turbine due to high thermal load applied on the steam turbine blade (STB) in cyclic form. The source of thermal cyclic load is coming from high temperature and pressure steam supplied to steam turbine blades. The steam supplied to turbine has cyclic action in each start-up of turbine. This

high thermal load causes high cyclic fatigue failure, which affects life of the blade. To detect the blade failure there are two mechanisms: experimental testing of failed blade and predicting the failure life using different software packages. There are several methods have been devised to simulate steam flows, with different levels of complexities and accuracy. The simplest and most popular approach is the Navier-Stoke equations. This approach uses conservation laws of physics for mathematical modeling [8, 9]. Thermal fatigue failure occurs because of high temperature and pressure on the turbine blade. To determine temperature distribution on the blade use Navier-Stoke equations for mathematical modeling and CFD commercial code (ANSYS CFX) software. The main purpose of this thesis is to predict the life of steam turbine blade through analysis of its thermal fatigue using computational fluid dynamics software packages. This thermal stress is occurred due to transient temperature and pressure distribution on the blade [10]. To achieve the objectives of this research applying all the required procedures starting from literature review, mathematical modeling for CFD analysis using Navier-Stoke equations, 3D modeling of the blade using Solid Work 2018 and fatigue analysis using ANSYS workbench 19.0. Finally predict the life of steam turbine blade due to thermal load.

1.3 Statement of the problem

There are different industries in Ethiopia. From those industries, Finchaa sugar factory is the oldest in production of sugar and ethanol in good qualities. The factory uses electric power for their different machine and household from electric power generated in steam turbine plant. The way of electric generation in this factory is using high-pressure steam as prime mover from boiler plant through the rotation of turbine shaft due to high pressure applied on the steam turbine blades, which is coupled to the rotor of generator. Turbine blades are the basic components of a steam turbine. As the steam is repeatedly applied to the blades, thermal fatigue failures occur which affect the life of the steam turbine blades, leading to the system shutdown. There are different factors that leads turbine blade for fatigue failures like corrosion fatigue failure, fretting fatigue failure and thermal fatigue failure. [11]. The main problem occurred on steam turbine blade is due to thermal fatigue failure which is depend on the thermal properties of steam. Finchaa Sugar Factory takes annual maintenance for different machines, but foreign engineers and technicians do internal steam turbine maintenance once per four years. Therefore, the objective of this study is to address the problem of steam turbine blade fatigue failure by predicting the more precise fatigue life of the blade. Stress-life (S-N) high cyclic fatigue analysis approach to predict the more accurate expected fatigue life of the steam turbine blade.

1.4 Objectives of the Study

1.4.1 General Objective

The general objective of this research is to predict the life of steam turbine blade through analysis of its thermal fatigue using fluid structure interaction coupling approach.

1.4.2 Specific Objectives

The specific objectives of study include:

- To determine temperature and pressure distribution of the steam turbine blade using computational fluid dynamics (CFD) software packages.
- To analyze stress distribution of the steam turbine blade.
- To predict life of steam turbine blade.

1.5 Scope and limitation of the Study

1.5.1 Scope of the study

The scope of this study is constrained to predict the fatigue life of steam turbine blade. To predict the life of steam turbine blade (STB) fatigue analysis is conducted which is caused due to thermal load effect.

In general, this study is focused on:

- This study is focus on fatigue failure of steam turbine blade operates in Finchaa Sugar Factory.
- This study consists of Fluid Structure Interaction (FSI) approach for determination of thermal distribution and stress distribution in the steam turbine blade.
- The study covers estimating the life of turbine blades considering the fatigue effect because of the variable temperature and pressure distribution.

1.5.2 Limitation of the study

The major limitation while conducting this study were the followings;

- Low capacity of the computer to handle large simulation process.
- Due to lack of sufficient laboratory, the results are not verified by experimental results.

- Only considering thermal load for fatigue failure
- The other limitation is handling two-way fluid structure interaction.

1.6 Significance of the Study

The idea of save-life is very important in the industrial machine operations. Analyzing the failure of the machine before failure/fracture occur is essential to save operator of the machine from injury and the machine from shut down operation. The researcher estimates the fatigue life of steam turbine blade in Finch Sugar Factory before it fractured due to thermal fatigue loads. In addition, this research document can be used as a reference for other researchers who wants to study on this area.

1.7 Research Methodology

The study frame of this research is formulated as follows to achieve the objective of the research.

- Review different scientific papers, journal articles, conference papers, books and thesis that done on the fatigue failure of steam turbine blade. The review of literature's are mainly focuses on the causes of fatigue failure that occurs on the steam turbine blades, identifying the variables that affect the fatigue failures and the effect of thermal fatigue on the life of steam turbine blade.
- To model and analyze fatigue failure of steam turbine blade (STB) input data is necessary. Those data are collected from FSF and literature, data collected from Finchaa Sugar Factory is, inlet and exit pressure, inlet and exit temperature, flow rate of the steam and type of steam turbine used in the factory is collected as primary data from Finchaa Sugar Factory electric power generation plant. Moreover, data collected from literature's are blade dimension and mechanical properties of blade material based on steam turbine model that applicable in Finchaa Sugar Factory.
- Mathematical equation was developed for computational fluid dynamics (CFD) using partial differential equation form of Navier-Stokes equations and for static structural analysis using stress-life methods.
- Three-dimensional modelling of steam turbine blade is demonstrated by Solid Work V2018 software packages. To model 3D of steam turbine blade (STB) the dimensions are taken from secondary data based on the steam turbine model applicable in Finchaa

Sugar Factory.

- Analyze the pressure and temperature distribution on steam turbine blade (STB) using computational fluid dynamics software packages (ANSYS Workbench 19.0). In analyzing computational fluid dynamics (CFD) of the blade, consider the boundary condition and mechanical properties of blade from collected data on the steam turbine blade that applicable in Finchaa Sugar Factory.
- ANSYS Workbench 19.0 using output temperature distribution from CFD analysis analyzes the static structural analysis of steam turbine blade.

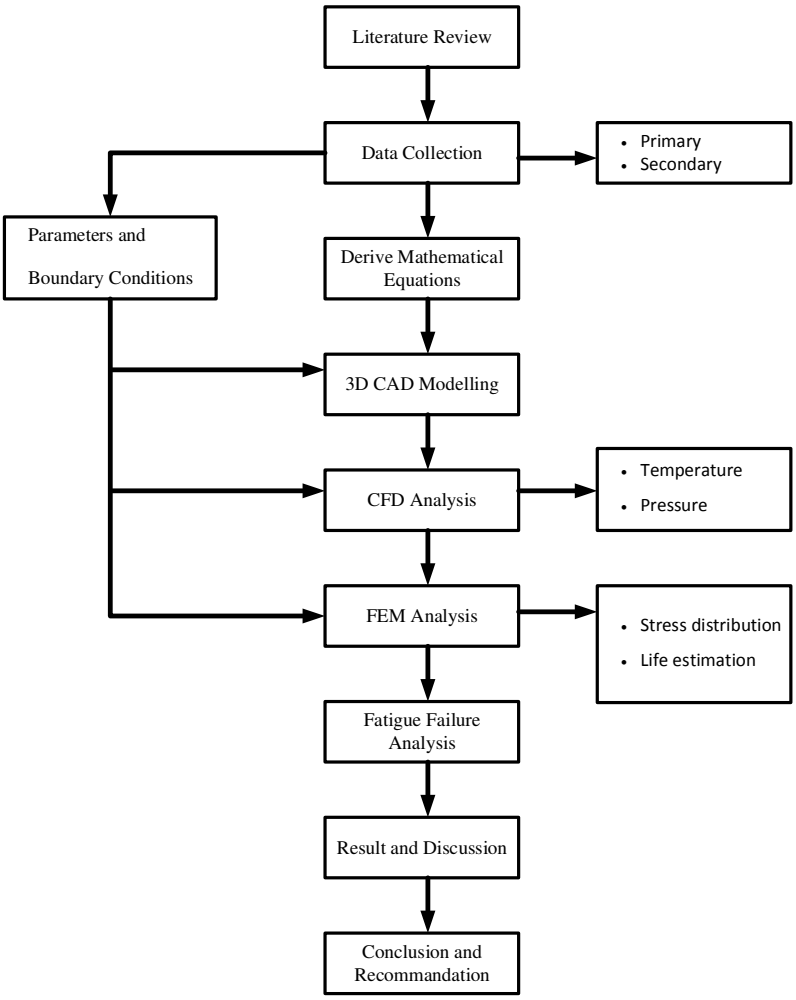

Figure 1.2: The schematic work flows of the thesis

1.8 Organization of the study

This thesis is organized in six chapters and the contents of each chapter is briefly outlined as follows.

In chapter one all the titles explained above is included under this chapter.

Chapter 2 contains the literature's related to fatigue analysis of steam turbine and the background of steam turbine are reviewed.

Chapter 3 presents the theoretical and mathematical approach of FSI. Under this chapter the mathematical modeling for CFD and structural dynamics are governed. In addition to this, the approach of fatigue analysis and fatigue criteria is discussed as well.

Chapter 4 provides the material used for steam turbine blade with specific properties are illustrated. In addition to this the methodology or setup of ANSYS Workbench are included.

Chapter 5 explained the result taken from the software. In addition, give a brief discussion.

Finally, the conclusion and recommendation are explained including the future works.

Chapter 2

LITERATURE REVIEW

This chapter provides a review of the literature on historical outlook, types of fatigue failure and fatigue life of steam turbine blade. The main purpose of this literature review is to get knowledge for academic and research areas that are related to the topic studied.

2.1 Turbine

A turbine is a rotary engine that extracts energy from a fluid flow and converts it into useful work. The simplest turbines have one moving part, a rotor assembly, which is a shaft or drum with blades attached. Moving fluid acts on the blades, or the blades react to the flow, so that they move and impart rotational energy to the rotor.

2.1.1 Types of turbine

Turbines are classified based on working fluids: Steam turbine, Gas turbine, Wind turbine and Hydro turbine (like Pelton turbine, Francis turbine, Kaplan turbine, Voith, water turbin). In wind turbine there is no casing to cover the rotating blade because it is exposed to the working fluid. Nevertheless, in gas, steam, and water turbines usually have a casing around the blades that contains and controls the working fluid.

2.1.2 Theory of operation

A working fluid contains potential energy (pressure head) and kinetic energy (velocity head). The fluid may be compressible or incompressible.

A. Impulse turbines

These turbines change the direction of flow of a high velocity fluid jet. The resulting impulse

spins the turbine and leaves the fluid flow with diminished kinetic energy. There is no pressure change of the fluid in the turbine rotor blades. Before reaching the turbine, the fluid's pressure head is changed to velocity head by accelerating the fluid with a nozzle.

B. Reaction turbines

These turbines develop torque by reacting to the fluid's pressure or weight. The pressure of the fluid changes as it passes through the turbine rotor blades. A pressure casement is needed to contain the working fluid as it acts on the turbine stage(s) or the turbine must be fully immersed in the fluid flow (wind turbines).

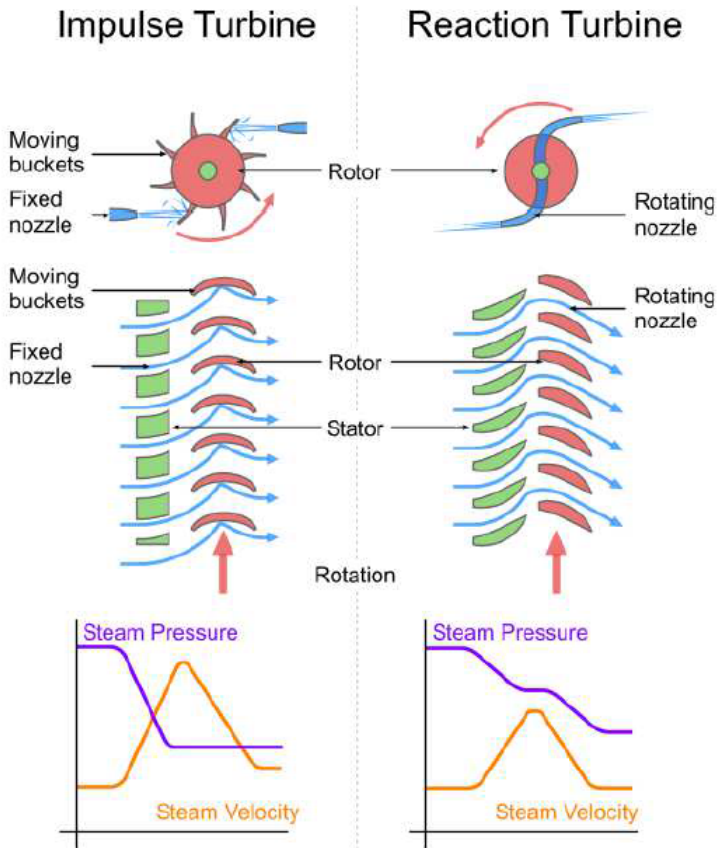

Figure 2.1: Schematic diagram outlining the difference between an impulse and a reaction turbine

2.1.3 Steam turbine

A steam turbine is a mechanical device that extracts thermal energy from pressurized steam, and converts it into rotary motion. The first steam turbine was invented by Greek mathematician Hero of Alexandria in Roman Egypt, which is called the Aeolipile, a hollow sphere supported on two brackets on the lid of a basin of boiling water. One bracket was hollow and conducted steam [12]. In Herons turbine, the steam makes the rotor react to the force the steam exerts upon it when the steam is forced to change direction, and it is called a reaction turbine [13]. Another similar rudimentary steam turbine is shown by Giovanni Branca, he is an Italian en-

Figure 2.2: Herons idea for a steam turbine

gineer, in 1629 for turning a cylindrical escapement device that alternately lifted and let fall a pair of pestles working in mortars. The steam flow of these early steam turbines, however, was not concentrated and most of its energy was dissipated in all directions. This would have led to a great waste of energy and so they were never seriously considered for industrial use [14]. In Brancas proposal, the steam is given a high velocity and then flows tangentially into the turbine wheel, acting on the blades. Hence, this is called an action or impulse turbine. The gear wheels drive a stamping mill not shown in the figure 2.3 [12, 13]. The modern steam turbine was in-

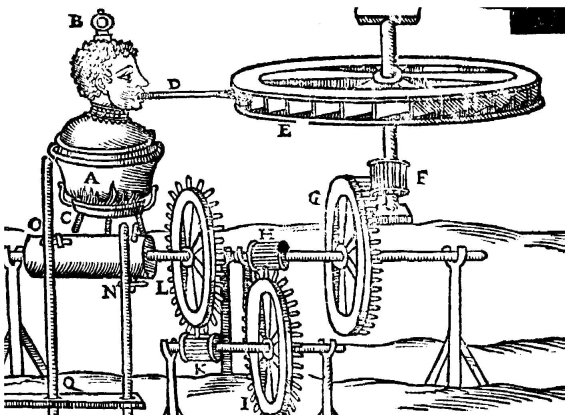

Figure 2.3: Brancas conceptual study of an action turbine

vented in 1884 by the Englishman Sir Charles Parsons, whose first model was connected to a dynamo that generated 7.5kW (10hp.) of electricity [12]. The invention of Parsons' steam turbine made cheap and plentiful electricity possible and revolutionized marine transport and naval warfare Parsons' design was a reaction type. His patent was licensed and the turbine scaled-up shortly after by an American, George Westinghouse. Figure 2.4 illustrate that the parson tur-

bine from the polished destroyer ORP Wincher [15]. In recent time, the use of steam turbine

Figure 2.4: Parsons turbine from the Polish destroyer ORP Wincher

for electric generation is more dominant in the world. To increase the efficiency of the turbine many scientists spent their time and knowledge in design and development of different steam turbine components. The major steam components are classified as internal and external components. Major internal components are Rotating Blading (Buckets), discs/wheels, Shafts, Rotor, Bearing, Seals, Stationary Blading (Nozzles), Diaphragms, Shells, blade rings and casings. Major external Components/Supporting Systems are: Main Stop, Trip, Throttle, Intercept Valves, Governor/Control Valves, Admissions, Extraction, Non-Return Valves, Steam, Drain Connections, over speed Protection System, Lubrication System, Electro-hydraulic Control System, Water/Steam Chemistry Controls, and Turbine Control System [11]. Rotating Blading (Buckets) are internal component of steam turbine, which is assembled to rotating shaft by blade disc. This blade is directly exposed to high-pressurized steam in high temperature. This high temperature creates thermal load on the blade, which is the responsible for thermal fatigue failure. Unless fatigue failure of steam turbine blade is analyzed earlier steam turbine, disaster occurs in the factory. Steam turbine is classified depend upon the behavior of steam in vicinity of the blades. Steam turbines are divided into two major classes: impulse turbine and reaction turbine.

2.2 Failures of Steam Turbine Blade

Turbine blades are subjected to very active environments inside a steam turbine. They face high temperatures, high stresses, and high vibration environment. All three of these factors can lead to blade failures, which can destroy the turbine. Generally, there are various factors causing failures of turbine blade. However, the factors which significantly influence the blade life time are as follows [11]:

- Corrosion failure

- Fretting fatigue failure
- Thermal fatigue failures

2.2.1 Corrosion Failure

A corrosion failure occurs due to chemical reactions, when the metal is mainly oxidized, if it is unprotected from oxygen, when the metals are wears away, and if it is exposed to external loads. Corrosion is accelerated by high temperatures and unpurified water in steam generation. From steam turbine pressure distribution, low pressure (LP) turbine blades are generally more susceptible to failure than those of the high pressure (HP) and intermediate pressure (IP) as discussed in [6, 16] [17]. The large capacity steam turbine at low-pressure stage is difficult to manufacture and implementation, because of many problems arises that cause the fatigue failure of turbine blade. Those problems are: corrosion fatigue, stress corrosion cracking, pitting, low cycle fatigue, and erosion-corrosion during the operation is presented in [5, 18] [19]. In previous investigations [19] conclude that, corrosion fatigue and stress corrosion cracking is the main cause of blade failure. In his non-distractive experimental investigation, fractography of the broken tang and cracked fillet of the blade root is carried out using stereomicroscope and scanning electron microscope (SEM), the fractured surface is observed. The report stated in [20] is done by the visual observation and metallurgical analysis of steam turbine blade. When the blade and disc is mismatched, there was high stress concentration is formed, the crack is initiated. He concludes that due to dynamic and static steam force, the crack is easily propagated and the blade is fractured at the end. Pitting corrosion has been detected at the first load-bearing flank of a low-pressure steam turbine blade during a major service. Metallographic investigations as well as qualitative finite element analysis (FEA) of the cracks were carried out to determine the root cause of the failure [18]. Linear elastic fracture mechanics (LEFM) is used to calculate the crack propagating stress range. In [17] investigation there are pit throughout the blade surface, silicon phase was detected. Several pits/grooves were found on the edges of the blades and chloride was detected in these pits, which was responsible for the crevice type corrosion. At this crevice, corrosion stress concentration is very high to cause crack propagation catastrophically. Inside the steam turbine, a Solid-particle erosion mechanism caused the deformation, cracking, cutting and detachment of the blade material producing wear grooves. This wear groove acted as stress raisers and promoted the nucleation of fatigue cracks is stated in [21] experiments. He suggested that, the fatigue cracks of the lower trailing edge grew preferentially during the transient regime of the steam turbine operation. Their fracture was the result of fatigue crack initiation

and propagation up to the formation of a critical crack on the blade [22] and concluding that the crack propagation started from leading edge as a part-through surface flaw produced by erosive and corrosive pitting effects. In the investigation of water drop erosion as a cause of failure of steam turbine blade in thermoelectric plant steam turbine generator (140 MV) non-destructive testing, microstructural characterization, chemical analysis, micro hardness and tensile testing do the experimental testing. This water drop erosion form a wear or groove at which stress is raised and nucleation of crack is formed and propagated [21]. Low-cycle fatigue cracking of steam turbine blade is mainly related to transient thermal stresses occurring during turbine start-ups and shutdowns. High thermal and mechanical loads generate stresses exceeding the material yield stress at stress concentration areas and their repetitive occurrence may lead to fatigue crack initiation and propagation [23]. Since the crack is happened due to low cycle fatigue, it has both elastic and plastic deformation that is called total strain range [24, 25].

2.2.2 Fretting Fatigue Failure

Fretting failures in steam turbine blade is occur due to blade/disk attachment at the fir tree joint. Although this joint is technically fixed, but at micro-scale relative movement at the interface between the blades and disks experience both centrifugal and oscillatory tangential movement vibrations resulting in damage and causes a significant reduction in fatigue life [11]. The damage and fracture in the blades joints are attributed to high vibrations stresses combined with high cycle fatigue during startup and shutdown of the turbine [26]. The research conducted by [20] conclude that the metallurgical mode of the blade root failure was the corrosion-fatigue at the zone of the highest stress concentration caused by mismatch and errors in the installation between the blade root platform and the disk fastening tree. In addition, the vibrations around of the first mode of vibration propagated the crack. Abnormal application of welding material modified the natural frequency of the blades leading to vibration in which resonance mode is happened and cause the blade failure/damage [27]. During the operation of the steam turbine, some components are in rotation, which form dynamic loads. In many cases, the blade failure is predominantly related to the vibration of turbine. The blade vibration is studied to analyze the natural frequencies and mode shapes of the blade, if the natural frequency is coinciding with the excitation frequency resonance is happened and then the blade is fractured.

2.2.3 Thermal Fatigue Failures

High temperatures are the main cause to yield high cycle fatigue failure in high-pressure turbine blade by propagating the crack. In order to study the fracture mechanism due to high cyclic fatigue failure it is necessary to compute the stress intensity factors in crack front [28] and stress concentration factor at the groove base of the blade is analyzed by FEA. Stresses due to thermal and dynamic loads of high pressure steam turbine blade of 210 MW power stations are analyzed in [29]. High thermal load is applied on the steam turbine blade as high thermal transient load and high steady state load in the mechanism of thermal fatigue and creep respectively. Those loads are the main cause to produce high cyclic fatigue failure in high-pressure turbine blade. The first stage rotor blade of the steam turbine are analyzed by [30] for the static and thermal stresses using ANSYS 15 software. The researchers are intended to reducing the stresses and increasing the fatigue life the blade under consideration of high temperature environment. To increase the fatigue life of the blade they use the technique of making holes along the blade span. The number of holes are seven with different size (2 mm, 3 mm, and 4 mm) are analyzed to optimize the size of the holes and gate the result of seven holes with 2 mm hole size is the optimum. The correlation of the stress range due to these temperature fluctuations has been established by carrying out the transient thermo-mechanical FE analysis [31]. Full conjugate heat transfer modeling for steam turbines in transient operations is conducted by [32] to validate and verify the experimental data and conjugate heat transfer (CHT) approach and predict the long-duration transient natural convection conjugate heat transfer problems of steam turbines in terms of computational efficiency and accuracy. Under the study of [33] a unified viscoplastic constitutive model with damage is presented to describe creepfatigue deformation behavior. The Creep and fatigue tests under different temperature and loading conditions were conducted to validate the material model. Those researchers are done on the 1000 MW rotor to the damage of rotor due to the combination of both creep and fatigue distribution through the analyses of mechanical properties of the rotor. A significant growth in creep damage was found under the influence of the temperature fluctuation compared to the creep damage under the stable temperature condition [31]. The results actually disclose that the combination of creep and fatigue deformation behavior further accelerate the damage. In the study of [34] the creep damage is analyzed by Norton model method and the modal analysis also performed. Based on the mechanical properties of steam turbine blade of high-pressure stage the static and dynamic properties of the blade is analyzed. Under static analysis the distributions of displacements, stress and strain components are performed. In addition, dynamic analysis of the interference

between frequencies of excitation and the natural frequencies was assessed.

2.3 Research Gap

Several researchers have identify three main cause of steam turbine blade fatigue failure namely corrosion fatigue failure, fretting fatigue failure and thermal fatigue failure.

- Some have proposed, traditional failure criteria, which depends on maximum stress or strain energy density, but these can not justify failures of many structures occurred at stress levels lower than the ultimate strength of the material.
- In thermal fatigue failure, some have proposed only consider Direct Numerical Simulation or Reynold Average Navier Stoke method in FSI turbulence simulation modeling but these cannot clearly indicate the small-scale turbulent flow.
- Some other researchers have used that in solid structure FEM modeling only consider mass and spring system but these can not justify solid dynamics modeling unless it include damping system.
- Effective steam turbine blade life predictions require computational tools and mathematical model that can accurately simulate the effect of fluid flow over solid structure using one-way FSI approach.
- Therefore, the objective of this study is to address this problem of steam turbine fatigue failure.

Chapter 3

THEORETICAL AND MATHEMATICAL APPROACH

This chapter deals with theoretical explanation for both fluid structure interaction and fundamentals of fatigue. In addition, governing equation of both fluid and solid part within their interfacing is derived.

3.1 Fluid-Structure Interaction (FSI)

Fluid-structure interaction occurs when fluid flow interacts with solid structures or bodies. The fluid and structure interact with each other by applying equal and opposite forces at the interface, satisfying physical boundary conditions (we use no-slip, no penetration boundary conditions) in the process. This fluid flow may interact solid bodies internally or externally. There are two main approaches to simulate FSI: monolithic (fully coupled) and partitioned (staggered) approach. The numerical discretization is also of great importance in FSI, especially at the interface surface. One option is to discretize the fluid and the solid systems together, which can be solved using a so-called monolithic approach (fully coupled). The governing equations of the fluid and solid are solved together. This requires a conformal mesh with matching nodal positions between the fluid and solid meshes. This system is very robust but requires a fully integrated FSI solver. A partitioned (staggered) approach is apply when the equations governing the fluid flow and the displacement of the structure are solved separately with two distinct solvers. The partitioned approach treats the fluid and the structure as two computational fields, which can be solved separately with their respective mesh discretization and numerical algorithm. Under partitioned approach, there are two cases: the first one is when the fluid is applied

on a solid structure; the deformation of this structure is enough to change the fluid flow itself. These means there is both direction interaction, which is called 2-way interactions. The other case is when the solid structure is not deformed the fluid flow is not changed. These means there is unidirectional interaction, which is called 1-way interaction. 2-way interaction partitioned algorithms use subsequent solutions of the fluid and structure sub-problems and the interaction is either loosely (explicitly) or strongly (implicitly) coupled. A loosely coupled algorithm is explicit and the codes will have only one bidirectional exchange of solved variables per time step, in a sequentially staggered manner and no iteration between fluid and solid field. A strongly coupled algorithm (implicit) uses an iterative staggered scheme which performs sub-iterations over the single fields to converge at the end of the time step.

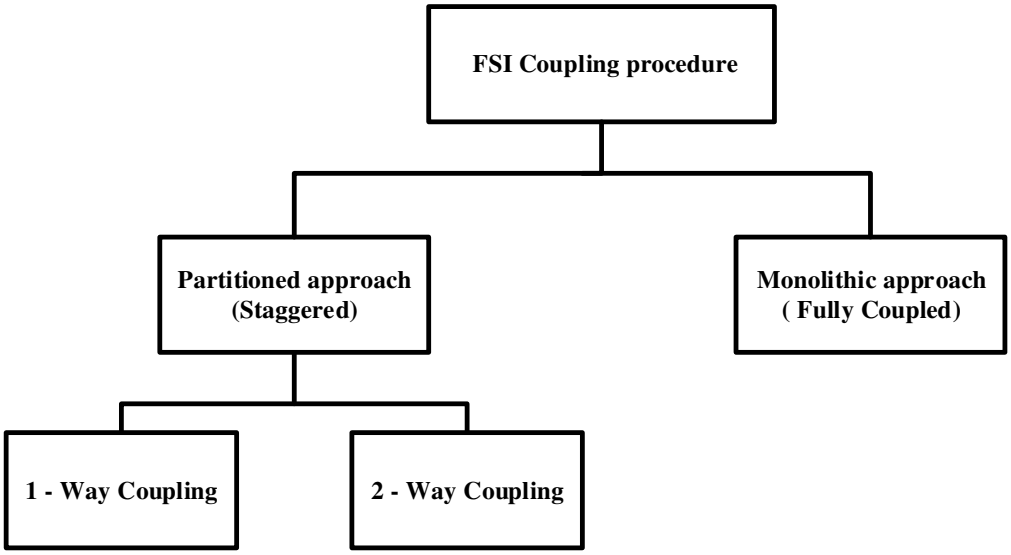

Figure 3.1: Solving / Coupling procedures in FSI

3.2 Computational Fluid Dynamics Analysis

Computational Fluid Dynamics (CFD) provides a qualitative and sometimes even quantitative prediction of fluid flows by means of mathematical modeling (partial differential equations), numerical methods (FDM, FEM and FVM) and software tools. The mathematical modeling of the steam is based on conservation laws of physics: mass conservation, momentum conservation and energy conservation, which are derived in the form of partial differential equations. Equation of state for thermodynamic equilibrium are derived as linear algebra by considering the steam as perfect gas. Considering the boundary condition as a part of mathematical modeling. The Finite Volume Method (FVM) is a numerical technique that transforms the partial

differential equations representing conservation laws over differential volumes into discrete algebraic equations over finite volumes (or elements or cells). Because the flux entering a given volume is identical to that leaving the adjacent volume, the FVM is strictly conservative. This inherent conservation property of the FVM makes it the preferred method in CFD. These characteristics have made the Finite Volume Method quite suitable for the numerical simulation of a variety of applications involving fluid flow and heat and mass transfer, and developments in the method have been closely entwined with advances in CFD [35, 36] [37]. Software tool to analyze CFD used is ANSYS Workbench 19.0. CFD Package contain three main elements process: (i) Pre-processor, (ii) Solver and (iii) Post-processor. The detail of these processes are shown in schematic diagram form as figure 3.2

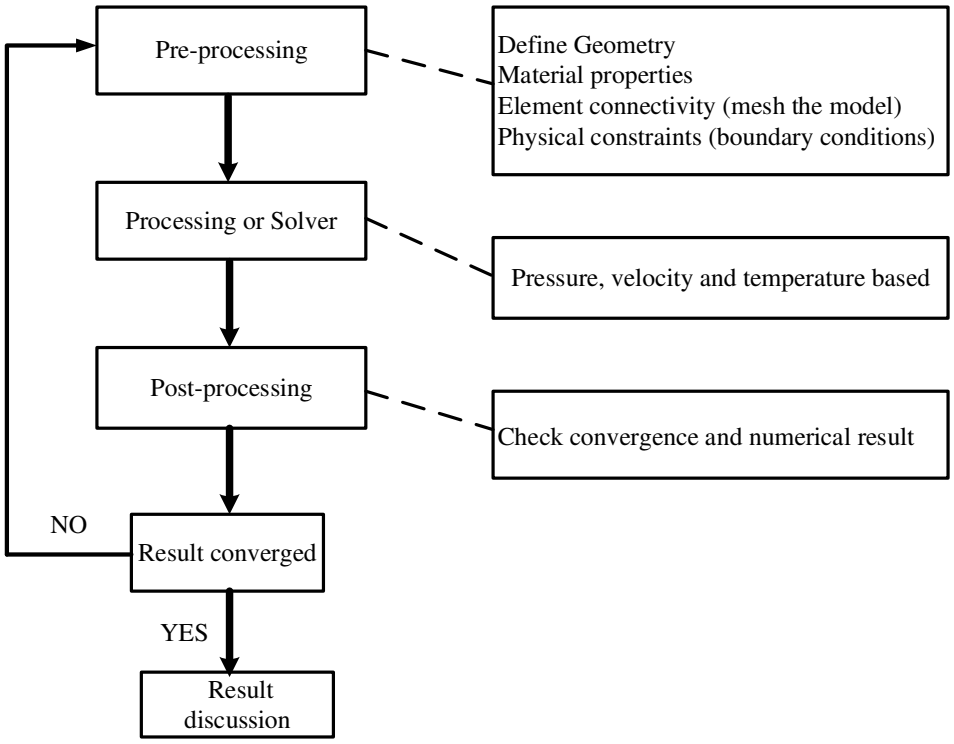

Figure 3.2: Schematic procedure of CFD analysis

3.3 Governing Equation of fluid

Mathematical modelling in this context mean that representing steam flow in the turbine as partial differential equations. The computational domain of the CFD analysis of steam flow is control volume using the numerical discretization method of finite volume method (FVM) on Cartesian space system. The steam is considered as unsteady, compressible, viscous and Newtonian fluid. The governing equations of steam flow represent mathematical statements of the conservation laws of physics. Those conservation's are as follows:

- The mass of a steam is conserved.
- The rate of change of momentum equals the sum of the forces on a steam particle (Newtons second law).
- The rate of change of energy is equal to the sum of the rate of heat addition to and the rate of work done on a steam particle (first law of thermodynamics).

The behavior of the steam is described in terms of macroscopic properties, such as velocity, pressure, density and temperature, and their space and time derivatives. Conservation form of Favre-Averaged Navier-Stokes System of Equation The Favre-Averaged Navier-Stokes equations in integral form is derived from the basic conservation equations applied to properties of fluids. In order to derive Navier-Stokes equations, apply the equation of conservation of mass, momentum and energy, and finally combine in to single equation.

3.3.1 The Navier-Stokes Equations

The Navier-Stokes equations can be used to entirely describe any compressible turbulent flow, in the continuum regime, and in the absence of external forces. These equations express the conservation of mass, momentum and energy and finally read as:

$$\frac{\partial \rho}{\partial t} + \frac{\partial \rho u_i}{\partial x_i} = 0 \tag{3.1}$$

$$\frac{\partial \rho u_i}{\partial t} + \frac{\partial}{\partial_{x_j}} \left[\rho u_i u_j + P\delta_{ij} - \tau_{ij} +\right] = 0 \tag{3.2}$$

$$\frac{\partial \rho E}{\partial t} + \frac{\partial}{\partial_{x_j}} \left[(P + \rho E)u_j + q_j - u_i \tau_{ij} +\right] = 0 \tag{3.3}$$

Here, ρ is the density, $(u_i)i = 1, 2, 3$ is the velocity vector in Cartesian coordinates, P is the pressure. The total energy is noted E, and τ_{ij} the stress tensor, q_j the heat flux vector. The total energy is the sum of internal energy (e) and kinetic energy:

$$E = e + \frac{1}{2} u_k u_k \tag{3.4}$$

Equation of State (EOS)

It is assumed in the present study that the gases under consideration obey to the perfect gas EOS. Introducing the temperature T, this EOS can be expressed as:

$$P = \rho RT \tag{3.5}$$

Here, R is the universal gas constant per unit mass.

Definition of the stress tensor

The fluids simulated here are assumed to be Newtonian: the stresses are proportional to the local rate of strain. Mathematically, this is expressed as:

$$\tau_{ij} = \mu \left(\frac{\partial u_i}{\partial x_j} + \frac{\partial u_j}{\partial x_i} \right) + \lambda \frac{\partial u_k}{\partial x_k} \delta_{ij} \tag{3.6}$$

Where μ is the viscosity coefficient, assumed to be a function of temperature only and λ is the bulk viscosity. Following Stokes hypothesis, it is assumed that the stress tensor is traceless, so that the bulk viscosity is related to μ as $\lambda = -\frac{2}{3}\mu$. Finally, the stress terms are given by:

$$\tau_{ij} = 2\mu \left(S_{ij} - \frac{1}{3} S_{kk} \delta_{ij} \right) \tag{3.7}$$

Where, S_{ij} the rate of strain tensor:

$$S_{ij} = \frac{1}{2} \left(\frac{\partial u_i}{\partial x_j} + \frac{\partial u_j}{\partial x_i} \right) \tag{3.8}$$

Definition of the heat flux vector

The heat flux vector has contributions from the thermal conduction and from the flux of sensible enthalpy due to species diffusion. Fourier's law is used to relate the thermal conduction to the local temperature gradient. The expression for the heat flux vector is:

$$q_i = -k \frac{\partial T}{\partial x_i} \tag{3.9}$$

Here, k the thermal conductivity is also a function of the temperature only

3.3.2 Turbulence simulation

Turbulent flows are entirely described by the Navier-Stokes equations, which involve a very large range of time- and length- scales. In addition, it can be encountered in nature and because of the work of man, such as a river or the smoke from a chimney. The study of such flows is important for aeronautics, meteorology and engineering, among others. The Reynolds number

$$R_e = \frac{LU}{v} = \frac{L\rho U}{\mu} \tag{3.10}$$

$$R_e = \frac{L\rho U}{\mu} = \frac{0.2 \times 13.7585 \times 805.43}{0.0013} = 1.70485 \times 10^7$$

With characteristic velocity U, characteristic length L, kinematic viscosity v , density ρ and dynamic viscosity μ is a measure for the turbulence of a flow.

Analytical approaches turbulence simulation are very complicated to employ for complex flow systems or even in a case of a laminar flow. Therefore, with the development in computers and availability of more computational resources, a numerical simulation of fluid flows has proven itself as an alternative and effective approach to tackling the problems in turbulent flows. Over past decades, three main simulation strategies have emerged, namely Direct Numerical Simulation (DNS), Reynolds-Averaged-Navier-Stokes (RANS) and Large eddy simulation (LES).

- **Direct Numerical Simulation (DNS)**

The most exact approach to turbulence simulation is to solve the Navier-Stokes equations without averaging or approximation. The result is a single realization of a flow and is equivalent to a short duration laboratory experiment; this approach is called direct numerical simulation (DNS). As the Reynolds number increases, the range of existing eddy scales also gets larger and the need for more grid numbers is inevitable in order to resolve all the scales in the flow field, especially the smallest scales.

For a successful simulation, one typically needs to know what the smallest length, time and velocity scales are. This information is crucial in order to set space grid and time steps of adequate scales. This data can easily be acquired by applying Kolmogorov turbulence theory in advance. What ones want to extract form these data typically is the number of grid point and time steps necessary.

This limitation restricts DNS to relatively low Reynolds and usually simple geometries, such as channel flow or isotropic turbulence in a periodic box. Given the current computer power, using DNS is impractical for complex engineering flows such as those that occur in an internal combustion engine. Thus, it is apparent, for complex flows, a turbulence model is necessary to account for the unresolved scales.

- **Reynolds-Averaged-Navier-Stokes (RANS)**

In Reynolds averaged approaches to turbulence, all of the unsteadiness is averaged out; this means that all unsteadiness is regarded as part of the turbulence. The non-linear terms in the Navier-Stokes equations give rise to the Reynolds stress term in the Reynolds Averaged Navier-Stokes (RANS) equations. This term must be modeled if the equations are to be closed.

Considering the nature of turbulence, the observations reveal that, at a given point (or location) in the flow domain, a distinguished pattern is repeated more or less regularly in time. Due to this fact, it is possible to extract the average values of the flow variables such as velocity and

pressure in time and space. As the behavior of small scales (fluctuations) is not the subject of interest in some engineering applications, these small motions can be ignored over a range of specific time.

Two-equation models retain the Boussinesq eddy viscosity concept but use a partial differential equation for the turbulent kinetic energy k to determine the velocity scale. To obtain the dissipation and the length scale L, we note that in so-called equilibrium turbulent flows.

Kolmogorov [38] developed the first complete model of turbulence since it needs no prior information on turbulence characteristics. Kolmogorovs $k-\omega$ model requires the solution of two differential equations for kinetic energy (k) and specific dissipation rate ω. Subsequently, Wilcox introduced some modifications and improvements to Kolmogorovs $k-\omega$ model. Another version of the two-equation model was developed by Jones and Launder [39] known as the $k-\epsilon$ model. Apart from solving the k transport equation, this model also solves an equation for a dissipation rate. Launder and Sharma [40] developed a low-Reynolds version of the k-model.

- **Large eddy simulation (LES)**

Large-eddy simulation (LES) which was proposed in as early as 1963 by Smagorinsky. LES does not adopt the conventional time- or ensemble-averaging RANS approach with additional modelled transport equations being solved to obtain the so-called Reynolds stresses resulting from the averaging process. In LES the large scale motions (large eddies) of turbulent flow are computed directly and only small scale (sub-grid scale (SGS)) motions are modelled, resulting in a significant reduction in computational cost compared to DNS.

In large-eddy simulations (LES) large-scale motions are represented directly and smaller-scale motions are modeled. there are four conceptual steps:

1. The velocity u is split between a filtered component $\overline{u}$ and a residual (subgrid-scale) component $\acute{u} = u - \overline{u}$. The former represents the motion of large eddies.
2. In order to compute the evolution of the filtered velocity field, the filtered Navier-Stokes equations are derived from the Navier-Stokes equations (NSE). They have the same form as the unfiltered Navier- Stokes equations except a residual stress tensor arising from the residual motions.
3. The residual stress tensor has to be modeled in order to achieve closure of the equations.
4. The filtered equations are then solved numerically for the filtered velocity.

LES is more accurate than the RANS approach since the large eddies contain most of the turbulent energy and are responsible for most of the momentum transfer and turbulent mixing,

and LES captures these eddies in full detail directly whereas they are modelled in the RANS approach.

3.3.3 Governing Equations for LES

The Large Eddy Simulation equations are obtained by spatially filtering the Navier-Stokes equations, in order to separate the large, geometry-dependent scales from the small, universal scales. In the present section, a spatial filter is applied to the Navier Stokes equations, and the Favre-filtered LES equations are presented. All subgrid, unclosed terms are explicitly identified. LES is based on the definition of a filtering operation: a resolved variable, denoted by an overbar, is defined as [41].

Let $G(x, \acute{x})$ be the mathematical description of the filter Kernel used for this operation, where x and $\acute{x}$ are position vectors. Then, variable f is filtered into $\overline{f}$ as:

$$\overline{f}(x,t) = \int_D f(\acute{x},t)\, G(x,\acute{x})\, d^3\acute{x} \tag{3.11}$$

Where D represents the entire domain. Thus, the filter function determines the size and structure of the small scales. In compressible flows it is convenient to use Favre-filtering to avoid the introduction of SGS terms in the equation of conservation of mass. $\widetilde{f}$ is the Favre filtered variable f defined by:

$$\widetilde{f} = \frac{\overline{\rho f}}{\overline{\rho}} \tag{3.12}$$

Where ρ is the local fluid density.

3.3.4 Filtering the Navier-Stokes Equations

Applying the Favre-filtering operation to Navier-Stokes equations, we obtain the resolved transport equations.

- Mass conservation

The equation for mass conservation reads:

$$\frac{\partial \rho}{\partial t} + \frac{\partial \rho u_i}{\partial x_i} = 0 \tag{3.13}$$

Using the commutativity of the filter with the derivatives, the filtered continuity equation reads:

$$\frac{\partial \overline{\rho}}{\partial t} + \frac{\partial \overline{\rho u_i}}{\partial x_i} = 0 \tag{3.14}$$

Finally, in terms of Favre-filtered variables, this equation reduces to:

$$\frac{\partial \overline{\rho}}{\partial t} + \frac{\partial \overline{\rho}\widetilde{u}}{\partial x_i} = 0 \tag{3.15}$$

- Momentum conservation

The governing equation for the momentum is obtained by following the same steps as for the continuity equation: the exact equation is filtered, and the commutative of the filter with the derivatives is called. Finally, Favre-filtering is used. The governing equation for momentum reads:

$$\frac{\partial \overline{\rho}\widetilde{u_i}}{\partial t} + \frac{\partial}{\partial_{x_j}}\left[\overline{\rho}\widetilde{u_i u_j} + \overline{P}\delta_{ij} - \overline{\tau_{ij}}\right] = 0 \tag{3.16}$$

This relation is strictly equivalent to the following:

$$\frac{\partial \overline{\rho}\widetilde{u_i}}{\partial t} + \frac{\partial}{\partial_{x_j}}\left[\overline{\rho}\widetilde{u_i}\widetilde{u_j} + \overline{P}\delta_{ij} + \tau_{ij}^{sgs} - \overline{\tau_{ij}}\right] = 0 \tag{3.17}$$

so that the convective term in the equation above can be treated from the resolved field, and the subgrid stress $\tau_{ij}^{sgs} = \overline{\rho}(\widetilde{u_i u_j} - \widetilde{u_i}\widetilde{u_j})$ is introduced.

- Energy conservation

The exact total energy equation is filtered into:

$$\frac{\partial \overline{\rho}\widetilde{E}}{\partial t} + \frac{\partial}{\partial_{x_j}}\left[\overline{\rho}\left(\widetilde{u_j E}\right) + \overline{u_j P} + \overline{q_j} - \overline{u_i \tau_{ij}}\right] = 0 \tag{3.18}$$

which again is strictly equal to:

$$\frac{\partial \overline{\rho}\widetilde{E}}{\partial t} + \frac{\partial}{\partial_{x_j}}\left[\overline{\rho}\widetilde{u_j}\widetilde{E} + \widetilde{u_j}\overline{P} + \overline{q_j} - \widetilde{u_i}\overline{\tau_{ij}} + H_j^{sgs} + \sigma_j^{sgs}\right] = 0 \tag{3.19}$$

where the terms $H_j^{sgs} = \overline{\rho}\left(\widetilde{u_j E} - \widetilde{u_j}\widetilde{E}\right) + \left(\overline{u_j P} - \widetilde{u_j}\overline{P}\right)$ and $\sigma_j^{sgs} = -\left(\overline{u_i \tau_{ij}} - \widetilde{u_i}\overline{\tau_{ij}}\right)$

The total energy being the sum of a kinetic and an internal contribution, the Favre averaged total energy $\widetilde{E}$ is given by:

$$\widetilde{E} = \widetilde{e} + \frac{1}{2}\widetilde{u_k u_k} \tag{3.20}$$

$$\widetilde{E} = \widetilde{e} + \frac{1}{2}\widetilde{u_k}\widetilde{u_k} + \frac{1}{2}\left(\widetilde{u_k u_k} - \widetilde{u_k}\widetilde{u_k}\right) \tag{3.21}$$

$$\widetilde{E} = \widetilde{e} + \frac{1}{2}\widetilde{u_k}\widetilde{u_k} + k^{sgs} \tag{3.22}$$

Here, k^{sgs} denotes the unresolved, or subgrid part of the kinetic energy.

- Equation of state (EOS)

The perfect gas EOS is used throughout this study. Filtering this equation leads to:

$$\overline{P} = \overline{\rho RT} = \overline{\rho}\widetilde{RT} = \overline{\rho}\widetilde{R}\widetilde{T} \tag{3.23}$$

- Stress Tensor

The filtered stress tensor in the momentum equation is computed in analogy to the unfiltered Navier-Stokes equations as follows:

$$\overline{\tau_{ij}} = 2\widetilde{\mu}\left(\widetilde{S_{ij}} - \frac{1}{3}\widetilde{S_{kk}}\delta_{ij}\right) \tag{3.24}$$

where $\widetilde{S_{ij}}$ represents the rate of filtered strain.

- Heat Flux Vector

Similarly, the filtered heat flux vector and the filtered species diffusion velocity are computed as:

$$\overline{q_i} = -\widetilde{k}\frac{\partial\widetilde{T}}{\partial x_i} \tag{3.25}$$

3.3.5 Subgrid-Scale Modeling in LES

LES can be divided into three distinguished categories or approaches in the context of sub-grid scale (SGS) modeling, namely, the eddy-viscosity model, similarity model and mixed model where the last one is a combination of the former two models. The main goal in all these three approaches is to provide and implement an effective model to account for the majority of unresolved scales in the turbulent flow. Eddy viscosity models are more popular than other available models in the LES. This model is based on the Boussinesq assumption [42] in bridging the turbulent and molecular transports through a so called turbulent or eddy-viscosity which is an artificial viscosity. The unclosed terms in the momentum equation, the subgrid stresses τ_{ij}^{sgs} are then closed as:

$$\tau_{ij}^{sgs} = -2\overline{\rho}\mu_{sgs}\left(\widetilde{S_{ij}} - \frac{1}{3}\widetilde{S_{kk}}\delta_{ij}\right) \tag{3.26}$$

Here, μ_{sgs} is eddy viscosity

There are three basic SGS-eddy viscosity model Smagorinsky model, Wall-adapted local eddy-viscosity (WALE) model and dynamic Smagorinsky-Lilly model. The first SGS model or LES was proposed by Smagorinsky [43] based on the idea that the energy produced in resolved scales is equal to the energy dissipation on unresolved/small scales. The mechanism is such

that the large eddies carrying the major fraction of turbulent energy transfers this energy to smaller scales.

There are three basic SGS-eddy viscosity model Smagorinsky model, Wall-adapted local eddy-viscosity (WALE) model and dynamic Smagorinsky-Lilly model. Wall-adapted local eddy-viscosity (WALE) model is the first choice. This is an algebraic model like the Smagorinsky model, but overcomes some known deficiencies of the Smagorinsky model. The wall-adapted eddy viscosity model is formulated locally and uses the following equation to compute the eddy-viscosity:

$$\mu_{sgs} = \rho \left(C_w \Delta\right)^2 \frac{\left(S_{ij}^d S_{ij}^d\right)^{3/2}}{\left(\overline{S}_{ij}\overline{S}_{ij}\right)^{5/2} + \left(S_{ij}^d S_{ij}^d\right)^{5/4}} \tag{3.27}$$

Where S_{ij}^d denotes the traceless symmetric part of the square of the velocity gradient tensor:

$$S_{ij}^d = \frac{1}{2}\left(\overline{g}_{ij}^2 + \overline{g}_{ij}^2\right) - \frac{1}{3}\delta_{ij}\overline{g}_{kk}^2 \tag{3.28}$$

And where $\overline{g}_{ij}^2 = \overline{g}_{ik}\overline{g}_{kj}, \overline{g}_{ij} = \partial\overline{u}_i/\partial x_j$ and δ_{ij} is the kronecker symbol. The tensor S_{ij}^d can be rewritten in terms of the strain-rate and vorticity tensors in the following way:

$$S_{ij}^d = \overline{S}_{ik}\overline{S}_{kj} + \overline{\Omega}_{ik}\overline{\Omega}_{kj} - \frac{1}{3}\delta_{ij}\left(\overline{S}_{mn}\overline{S}_{mn} - \overline{\Omega}_{mn}\overline{\Omega}_{mn}\right) \tag{3.29}$$

Where the vorticity tensor Ω_{ij} is given by:

$$\overline{\Omega}_{ij} = \frac{1}{2}\left(\frac{\partial\overline{U}_i}{\partial x_j} - \frac{\partial\overline{U}_j}{\partial x_i}\right) \tag{3.30}$$

The main advantages of the WALE model are the capability to reproduce the laminar to turbulent transition and the design of the model to return the correct wall-asymptotic variation of the SGS viscosity. The constant C_w has been calibrated using freely decaying isotropic homogeneous turbulence: the default value is 0.5 and is available in CFX.

The stress tensor is often divided into two terms of interest in the general form of the Navier-Stokes equation. The two terms are the volumetric stress tensor, which tends to change the volume of the body, and the stress deviator tensor, which tends to deform the body. The volumetric stress tensor represents the force, which sets the volume of the body (namely, the pressure and viscous forces). The stress deviator tensor $\mathbb{T}$ represents the forces, which determine body deformation and movement, and is composed of the shear stresses τ on the fluid.

$$\sigma = \begin{pmatrix} \sigma_{xx} & \tau_{xy} & \tau_{xz} \\ \tau_{xy} & \sigma_{yy} & \tau_{yz} \\ \tau_{xz} & \tau_{yz} & \sigma_{zz} \end{pmatrix} = - \begin{pmatrix} P & 0 & 0 \\ 0 & P & 0 \\ 0 & 0 & P \end{pmatrix} + \begin{pmatrix} \sigma_{xx} + P & \tau_{xy} & \tau_{xz} \\ \tau_{xy} & \sigma_{yy} + P & \tau_{yz} \\ \tau_{xz} & \tau_{yz} & \sigma_{zz} + P \end{pmatrix}$$

$$= -P\boldsymbol{I} + \mathbb{T} \tag{3.31}$$

Where, $\boldsymbol{I}$ is identity matrix and pressure P is given by:

$$P = -\frac{1}{3}\left(\sigma_{xx} + \sigma_{yy} + \sigma_{zz}\right) \tag{3.32}$$

The time stepping scheme we first used was based on the idea of iterating the residuals of an implicit scheme [44, 45]. In order to solve

$$\frac{V dw}{dt} + R(w) = 0 \tag{3.33}$$

Where V is the cell area or volume, $R(w)$ is the space residual for the solution w, a second order accurate implicit scheme has the form

$$w^{n+1} = w^n - \frac{\Delta t}{2}\left[R\left(w^{n+1}\right) + R\left(w^n\right)\right] \tag{3.34}$$

The fourth order Runge-Kutta scheme is given as

$w^1 = w^0 - \frac{1}{2}\Delta t R(w^0)$

$w^2 = w^0 - \frac{1}{2}\Delta t R(w^1)$

$w^3 = w^0 - \frac{1}{2}\Delta t R(w^2)$

$w^4 = w^0 - \frac{1}{6}\Delta t \left[R(w^0) + 2R(w^1) + 2R(w^2) + R(w^3)\right]$

3.3.6 Governing Equation of solid

The structural equations for a mechanical system with a finite number of degrees of freedom are given by [46].

$$[M]\{\ddot{X}\} + [C]\{\dot{X}\} + [K]\{X\} = \{F(t)\} \tag{3.35}$$

Where $[M]$ is the mass matrix, $[C]$ is the damping matrix, $[K]$ the stiffness matrix, $\{X\}$ the vector of displacements, and $\{F(t)\}$ is the vector of the external forces.

These equations are of size (n x n) depending on the size of the system matrices. Assuming that the damping matrix is proportional to either the mass or stiffness matrix, the eigen solution at

the full space of the physical model can be written as

$$[[K] - \lambda[M]]\{X\} = 0 \tag{3.36}$$

The resulting eigenvalue and eigenvector are noted as $\omega_1, \{u_i\}$. The eigenvectors can be arranged in column fashion to form the modal matrix $[U]$. Typically, none of the eigenvectors is used to describe the system. The modal matrix is therefore rectangular and of size (n x m).
Using this notation and noting the eigenvalues can be assembled into a diagonal matrix, the eigen problem can be restated as

$$[K][U_1] = [M][U_1]\left[\omega_1^2\right] \tag{3.37}$$

Using the modal matrix, a transformation can be made from physical space to modal space using the relationship

$$\{X\} = [U_1]\{p_1\} \tag{3.38}$$

Substituting this into the equation of motion and pre-multiplying by the transpose of the projection operator $[U_1^T]$ to put the equations into normal form gives the standard modal space representation

$$\left[U_1^T\right][M][U_1]\{\ddot{p}\} + \left[U_1^T\right][C][U_1]\{\dot{p}\} + \left[U_1^T\right][K][U_1]\{p\} = \left[U_1^T\right]\{F(t)\} \tag{3.39}$$

When equation of motion is written in the form of natural frequency and damping ratio as

$$\{\ddot{p}\} + 2\zeta\omega_n\{\dot{p}\} + \omega_n^2\{p\} = Q \tag{3.40}$$

$\left[U_1^T\right][M][U_1] = 1, \left[U_1^T\right][C][U_1] = 2\zeta\omega_n, \left[U_1^T\right][K][U_1] = \omega_n^2$ and $\left[U_1^T\right]\{F(t)\} = Q$ The second-order differential equation is transformed into two first-order equations using state space formation method.

$$\{\dot{X}\} = AX + B \tag{3.41}$$

$$x_1 = p_1$$

$$x_2 = \dot{p}_1$$

$$\dot{x}_1 = \dot{p}_1 = x_2$$

$$\dot{x}_2 = \dot{p}_1 = Q - 2\zeta\omega_n\dot{p}_1 - \omega_n^2 p_1$$

$$\begin{Bmatrix} \dot{x}_1 \\ \dot{x}_2 \end{Bmatrix} = \begin{bmatrix} 0 & 1 \\ -\omega_n^2 & -2\zeta\omega_n \end{bmatrix} \begin{Bmatrix} x_1 \\ x_2 \end{Bmatrix} + \begin{Bmatrix} 0 \\ Q \end{Bmatrix} \tag{3.42}$$

The discrete time at which the solution obtained $t_i = 1, 2, 3, ...x_{1,i}$ and $x_{2,i}$ is the displacements and velocities at these times. The recurrence relations for the simplest self-starting method, called the Euler method, are obtained from truncating Taylor series expansions.
These recurrence relations are

$$x_{1,i+1} = x_{1,i} + (t_{i+1} - t_i)\, x_{2,i} \tag{3.43}$$

$$x_{2,i+1} = x_{2,i} + (t_{i+1} - t_i)\left[Q - 2\zeta\omega_n x_{2,i} + \omega_n^2 x_{1,i}\right] \tag{3.44}$$

Runge-Kutta methods are more popular than the Euler method because of their better accuracy, while still being easy to use. A Runge-Kutta formula for the solution of the first order differential equation

$$\begin{gathered} \tfrac{d_x}{d_t} = \dot{x} = f(x,t) \\ x(t_0) = x_0 \end{gathered} \tag{3.45}$$

is of the form

$$x_{i+1} = x_i + \sum_{j=1}^{n} a_j K_j \tag{3.46}$$

Fourth order Runge-Kutta formula is given as below

$$x_{i+1} = x_i + \frac{1}{6}\left[K_1 + 2K_2 + 2K_3 + K_4\right] h \tag{3.47}$$

Where h is step size given in second and K is the slope at the beginning, midpoint and end of the interval.
$K_1 = f\left(t_i, x_i\right)$
$K_2 = f\left(t_i + \frac{1}{2}h, x_i + \frac{1}{2}K_1 h\right)$
$K_3 = f\left(t_i + \frac{1}{2}h, x_i + \frac{1}{2}K_2 h\right)$
$K_4 = f\left(t_i + h, x_i + K_3 h\right)$

3.3.7 Boundary conditions for compressible viscous flow

The boundary conditions acts as the constraints and established the uniqueness of the flow field for a specified problem. There are two types of boundary conditions: physical boundary condi-

tions that are imposed by physical processes at the boundary surfaces of the flow domain and artificial boundary conditions, which are specified at the boundaries of computational domain, which are not natural boundaries. Physical boundary conditions for a viscous flow, the velocity of the steam are equal to the velocity of the blade surface; this is called no-slip boundary condition. Moreover, temperature of the steam at the wall is equal to that of the blade wall.

$\overrightarrow{V} = V_m$ Where V_m is velocity of the blade surface (no-slip condition)

$T = T_w$ Where T_w is the temperature of the blade wall (fixed temperature) or

$K\partial T/\partial n = -q_w$ (Fixed heat flux at the wall)

Fluid boundary conditions have a variety form: inlet, outlet, symmetry, cyclic or periodic are the popular type. In case of this study since the steam, flow is compressible viscous flow only the inflow boundary is applied. These inlet parameters are mass flow rate, velocity, pressure and temperature as a function of position.Table 3.1 shows technical data of steam turbine taken from Finchaa Sugar Factory machine manual and specification as shown in APPENDIX A: A.

Table 3.1: Technical data of steam turbine

NAME	**DATA**
Type	Axial, impulse, non-condensing turbine
Serial number	D-3943
Turbine frame	S-6
Number of stage	7 (1-Curtis and 6-Rateau)
Output power	$3500KW$
Turbine rotation	Counterclockwise (CCW)
Inlet steam condition	
Pressure	$399psig$ = $27.51bar$ = $2.751MPa$
Temperature	$735°F$ = $390°C$ = $663k$
Mass flow rate	$8.95Kg/s$
Velocity	$805.43m/s$
Exhaust steam condition	
pressure	$18psig$ = $1.241bar$ = $0.1241MPa$
Temperature	$177^0C = 450k$
The 1^{st} critical speed	$2790rpm$
The 2^{nd} critical speed	$10000rpm$
Operating speed range	
Nominal	$5970rpm$
Maximum	$6269rpm$
Minimum	$5672rpm$

3.4 Fatigue Analysis

Preliminary understanding of metal fatigue failure developed during the industrial revolution in Europe during the 19th century as heavy-duty locomotives, boilers, etc. William Albert first published an article on fatigue that associated cyclic load with metal toughness. Who first named "fatigue" to this phenomenon was the English engineer Braithwaite in 1854, or possibly the French engineer and mathematician Poncelet, previously in 1839. Fatigue is a component failure after several cycles of repetitive load. After three stages of crack initiation (crack nucleation), crack propagation (crack growth) and failure, fatigue failure occurs. According to the ASTM definition, fatigue is a process of progressive localized permanent structural change occurring in a material subjected to conditions that produce fluctuating stresses and strains at a point or some points and that may culminate in cracks or complete fracture after a sufficient number of fluctuations. Based on cyclic load applied on the structures or solid bodies the load creates a strain imposed to elastic and plastic deformation. When the stress level is low and the deformation is primarily elastic, the fatigue is occurred as high cycle type. When the stress level is high enough for plastic deformation to occur, the fatigue is known as low cycle type.

3.4.1 Velocity triangle for impulse blade

Velocity triangle shows inlet and exit velocity with its relatives in one schematic. Since impulse steam turbine is the focus area of this study, which operates in Finchaa Sugar Factory, impulse velocity triangle are used to represent velocity. Figure 3.3 indicates velocity flow on the impulse turbine blade with their respective flow angle. The inlet mean velocity at steady state to turbine is $V_1 = 805.43m/s$, at angle flow of $\alpha_1 = 21.4^0$. The diameter of blade $D = 1.3085m$ and the speed of turbine is $N = 5970rpm$.

Peripheral speed of rotor blade at its midspan

$$U = \frac{\pi DN}{60} = \frac{\pi * 1.3085 * 5970}{60} = 409.02\frac{m}{s} \tag{3.48}$$

At the inlet of blade whirl velocity, flow velocity and relative velocity are calculated as equation (3.49), (3.50) and (3.51) respectively.

$$V_{w1} = V_1 \cos(\alpha_1) = 805.43 \cos(21.4^0) = 749.9\frac{m}{s} \tag{3.49}$$

$$V_{f1} = V_1 \sin(\alpha_1) = 805.43 \sin(21.4^0) = 293.88\frac{m}{s} \tag{3.50}$$

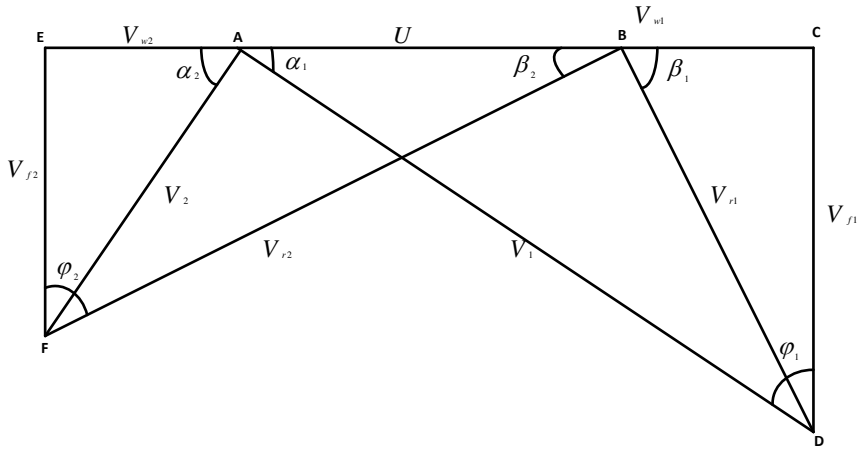

Figure 3.3: Velocity triangle for impulse turbine

$\overline{BC} = V_{w1} - U = 749.9 - 409.02 = 340.88\frac{m}{s}$

$$V_{r1} = \sqrt{\overline{BC}^2 + {V_{f1}}^2} = \sqrt{340.88^2 + 293.88^2} = 450.07\frac{m}{s} \tag{3.51}$$

At the exit of blade relative velocity, flow velocity, whirl velocity and relative flow angle are calculated as equation (3.52), (3.53), (3.54) and (3.56) respectively.

But for impulse blade

$$V_{r1} = V_{r2}, \qquad \text{therefore} \qquad V_{r2} = 450.07\frac{m}{s} \tag{3.52}$$

$\sin\beta_1 = \frac{V_{f1}}{V_{r1}} = 293.88/450.07 = 0.653, \qquad$ therefore $\qquad \beta_1 = \arcsin(0.653) = 40.7^0$

$\sin\varphi_1 = \frac{V_{w1}}{V_1} = 749.9/805.43 = 0.93, \qquad$ therefore $\qquad \varphi_1 = \arcsin(0.93) = 68.6^0$

Reaction is zero for impulse turbine $\tan\varphi_1 + \tan\varphi_2 = 0$; therefore φ_1 and φ_2 is equal but opposite in direction.

$\cos\varphi_2 = \frac{V_{f2}}{V_{r2}}, V_{f2} = V_{r2}\cos\varphi_2$

$$V_{f2} = 450.07\cos(-68.6^0) = 164.22\frac{m}{s} \tag{3.53}$$

$\overline{EB} = \sqrt{V_{f2}^2 + V_{r1}^2} = \sqrt{450.07^2 + 164.22^2} = 419.04\frac{m}{s}$

$$V_{w2} = \overline{EB} - U = 419.04 - 409.02 = 10.02\frac{m}{s} \tag{3.54}$$

$\cos\beta_2 = \frac{\overline{EB}}{V_{r2}} = \frac{419.04}{450.07} = 0.931, \beta_2 = \arccos(0.931) = 21.4^0$

$$V_2^2 = V_{f2}^2 + V_{w2}^2 \qquad \text{then} \qquad V_2 = \sqrt{V_{f2}^2 + V_{w2}^2} = \sqrt{164.22^2 + 10.02^2} = 27.07\frac{m}{s} \tag{3.55}$$

$$\cos(\alpha_2) = \frac{V_{w2}}{V_2} = \frac{10.02}{27.07} = 0.37 \qquad \text{then} \qquad \alpha_2 = \arccos(0.37) = 68.28^0 \tag{3.56}$$

Calculate tangential force (F_t) and axial force (F_a)

Tangential force: $F_t = \dot{m}(V_{w1} - V_{w2}) = 8.95(749.9 - 10.02) = 6621.93N$

Axial force: $F_a = \dot{m}(V_{f1} - V_{f2}) = 8.95(293.88 - 164.22) = 1160.46N$

Body forces, which are presented as forces per unit volume, may also arise due to a variety of effects. The force representing the weight of the material volume per unit volume in the presence of a gravitational field is denoted by gravitational force and given by

$$f_b = \rho \mathrm{g} \tag{3.57}$$

where g is the gravitational acceleration vector.

Therefore gravitational force is: $f_b = \rho \mathrm{g} = 13.7585 \times 9.81 = 134.97N$

Different load is applied on the blade that lead strain. Those loads are surface force occurred due to steam pressure and body force due to gravity. The other load is thermal load due to temperature. Thermal load applied to the blade creates thermal stress, which is a cause for thermal fatigue.

Stress due to temperature is given as:

$$\sigma = \frac{E\alpha \triangle T}{1 - v} \tag{3.58}$$

Super alloy Stainless steel is an isotropic material and it obeys Hookes law, which states that the stresses due to load are directly proportional to the strain produced due to deformations. In mathematical form shown as follows:

$$\begin{Bmatrix} \sigma_{xx} \\ \sigma_{yy} \\ \sigma_{zz} \\ \sigma_{yz} \\ \sigma_{zx} \\ \sigma_{xy} \end{Bmatrix} = \frac{E}{v+1} \begin{bmatrix} \frac{1-v}{1-2v} & \frac{v}{1-2v} & \frac{v}{1-2v} & 0 & 0 & 0 \\ \frac{v}{1-2v} & \frac{1-v}{1-2v} & \frac{v}{1-2v} & 0 & 0 & 0 \\ \frac{v}{1-2v} & \frac{v}{1-2v} & \frac{1-v}{1-2v} & 0 & 0 & 0 \\ 0 & 0 & 0 & 1 & 0 & 0 \\ 0 & 0 & 0 & 0 & 1 & 0 \\ 0 & 0 & 0 & 0 & 0 & 1 \end{bmatrix} \begin{Bmatrix} \varepsilon_{xx} \\ \varepsilon_{yy} \\ \varepsilon_{zz} \\ \varepsilon_{yz} \\ \varepsilon_{xz} \\ \varepsilon_{xy} \end{Bmatrix} \tag{3.59}$$

Figure 3.4 illustrate that the loading pattern on steam turbine blade in three different stage (start-up, operating and shut-down). During start-up and shut-down time the blade is slowly loaded for 10 minute and for 30 minute the rotational speed is 2790 rpm. The operating rotational speed of steam turbine is 5970 rpm for nine months except emergence shutdown happened on the turbine.

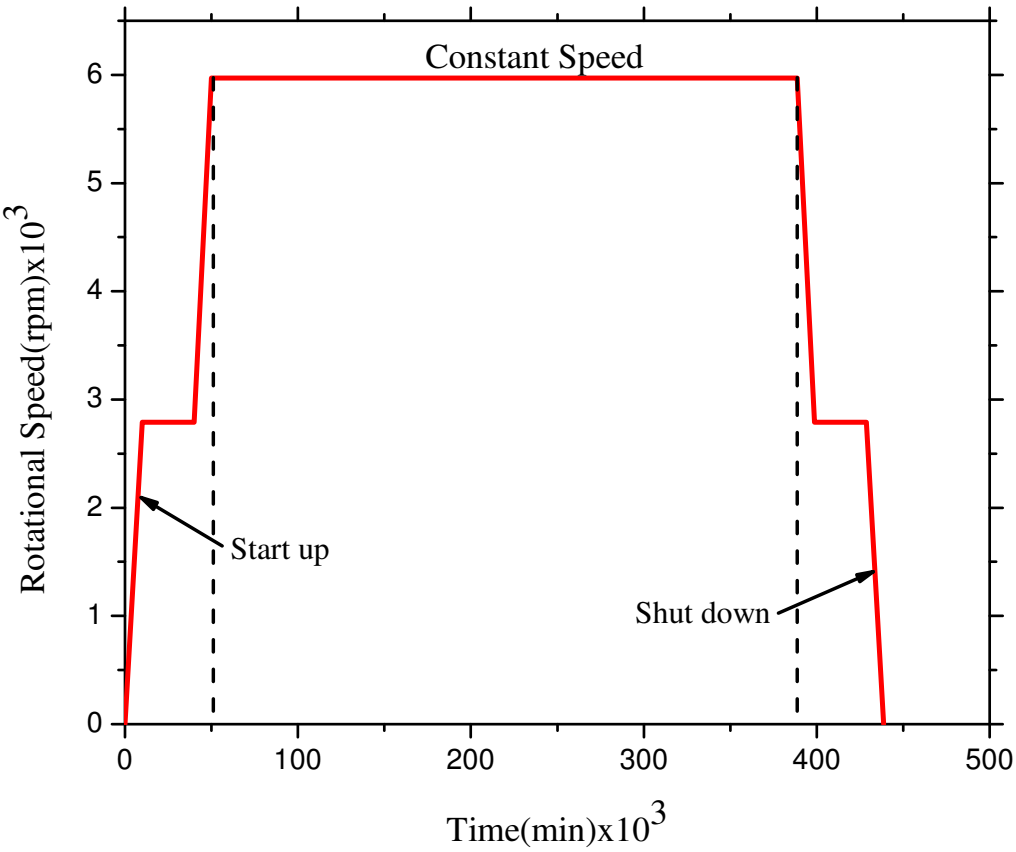

Figure 3.4: Blade loading pattern for fatigue life

3.4.2 Fatigue Analysis Approaches

The fatigue life of a member or of a structural detail subjected to repeated cyclic loading is defined as the number of stress cycles it can stand before failure. To analyze fatigue life there are three basic approaches: (i) stress-life (S-N) approach for high cyclic fatigue, (ii) strain-life (e-N) approach for low cyclic fatigue and (iii) linear elastic fracture mechanics (LEFM).

Basic terminology of fatigue analysis

There are different cyclic load mechanism applied on the structure or solid bodies as illustrated in figure 3.5.

The influence of local mean stress can be characterized as the influence of stress ratio, the ratio of a local minimum stress to a local maximum stress in a fatigue load cycle. For fully reversed

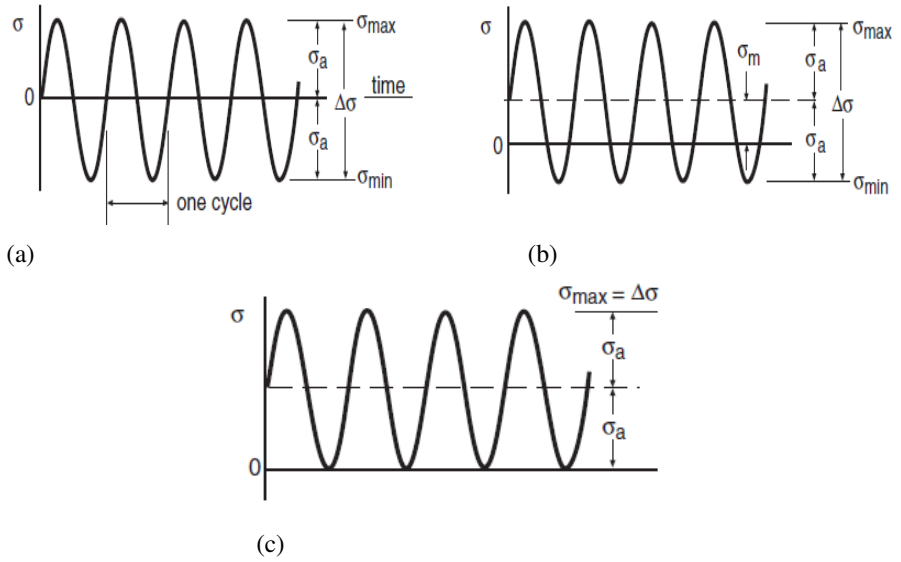

Figure 3.5: Constant amplitude cycling and the associated nomenclature. Fully reversed (a), fluctuated cyclic stresses (b) and repeated (c)

loading as represented in figure 3.5(a) the relation of parameters are stated as below [47].

Constant stress range: $\Delta\sigma = \sigma_{\max} - \sigma_{\min}$

Mean stress: $\sigma_m = \dfrac{\sigma_{\max} + \sigma_{\min}}{2}$

Stress amplitude: $\sigma_a = \dfrac{\Delta\sigma}{2} = \dfrac{\sigma_{\max} - \sigma_{\min}}{2}$

Stress ratio: $R = \dfrac{\sigma_{min}}{\sigma_{max}}$

Amplitude ratio: $A = \dfrac{\sigma_a}{\sigma_m}$

Maximum Stress: $\sigma_{max} = \sigma_m + \sigma_a$

Minimum Stress: $\sigma_{min} = \sigma_m - \sigma_a$

Where: σ_{max} Local maximum stress in a fatigue load cycle

σ_{max} Local minimum stress in a fatigue load cycle

Stress-Life (S-N) Theory

The stress-life (S-N) analysis estimates the time spent to initiate and grow a crack until the component breaks (failures) into parts. The stress-life curve is a graphical representation of fatigue data. It represents the relationship between fatigue life, in cycles, and the applied stress amplitude. Since steam turbine blade loaded by high thermal load, fatigue failure occurred is high cyclic, so stress-life (S-N) approach is used for fatigue analysis. German August Whler has developed this stress-life (S-N) curve for his systematic fatigue tests done in the 1870s [48]. The three basic strength of stress-life (S-N) approach:

- The analysis and estimation of material constants necessary for this method are quite simple. This allow quick back of the envelope calculations to get a reasonable estimate of life.

- This method works well for designs involving long life, constant amplitude histories.
- There are reams of data available for almost any variation in surface finish, long configuration, environment and so on.

Basquins relation the most commonly used model and provides an analytical expression of the S-N curve, for high cycle fatigue [47, 49]

$$\begin{gathered} \sigma_a = \acute{\sigma_f} \left(2N_f\right)^b \qquad \text{and} \qquad \sigma_a = \frac{\triangle\sigma}{2} = \frac{\triangle\varepsilon_e E}{2} \\ \frac{\triangle\varepsilon_e}{2} = \frac{\sigma_a}{E} = \left(\frac{\sigma_f^{'}}{E}\right)\left(2N_f\right)^b \qquad \text{then} \qquad N_f = \frac{1}{2}\sqrt[b]{\frac{\triangle\varepsilon_e E}{2\sigma_f^{'}}} \end{gathered} \tag{3.60}$$

$$b = \frac{\left(\log\left(S_e\right) - log\left(0.9S_u\right)\right)}{3} \tag{3.61}$$

Where $\sigma_f^{'}$: Fatigue strength coefficient (for most metals it is the tensile strength), b: Is the fatigue strength exponent or Basquin exponent (-0.05 to -0.12), slope of the log-log curve and N_f: Is the number of reversals to failure.

These coefficients can be evaluated by use least square method (linearizing the power law in logarithmic form), it is important to mention that the S-N curve is represented in the log-log scale. From equation (3.61) endurance limit $(S_e = 669MPa)$, Hardness Brinell $(HB) = 879.75MPa$ and ultimate strength $(S_u = 3.45HB = 879.75MPa)$. Then the value of fatigue strength exponent is -0.02439 and fatigue strength coefficient is $\sigma_f^{'} = 1235MPa$.

Therefore, stress amplitude function is given as:

$$\sigma_a = 1213.8(N_f)^{-0.02439} \tag{3.62}$$

Fatigue Life (N_f) is defined as the number of stress cycles or strain reversals that a material experiences prior to fracture. Generally, there are three crack stages: (i) crack initiation in the areas of stress concentration (near stress raisers), (ii) incremental crack propagation and (iii) rapid crack propagation after crack reaches critical size.

The total number of cycles to failure is the sum of cycles at the first and the second stages

$$N_f = N_i + N_p \tag{3.63}$$

Where N_f: Number of cycles to failure,N_i: Number of cycles for crack initiation and N_p: Number of cycles for crack propagation Generally, there are many theories used to study influence of the mean stress. The Goodman theory, the Soderberg theory, and the Gerber theory are basic

theories. In the analysis of fatigue life using S-N approach Goodman theory is a good choice for brittle material and used when negative mean stress is not bounded. Therefore, this study also use Goodman theory, which is given in equation (3.64).

$$\frac{\sigma_a}{\sigma_e} + \frac{\sigma_m}{\sigma_u} = 1 \tag{3.64}$$

Where σ_m: mean stress, σ_a: stress amplitude, σ_e : is the endurance fatigue limit, and σ_u : is the ultimate tensile strength,

3.4.3 Failure criteria

Many failure criteria are based on principal stresses rather than the standard engineering stress and strain. Principal stress is determined from the value of the engineering stress and strain at every point. In general there are four different failure criteria (i) Maximum Shear Stress Criterion (Trescas Hexagon), (ii) Maximum Distortion Energy Criterion (Von Mises), (iii) Maximum Normal Stress Criterion (Coulombs Criteria), (iv) Maximum Normal Strain Criterion (St. Venants Criteria) [50, 51].

Von Mises Stress failure criterion:

A given structural component is safe if the maximum value of the distortion energy per unit volume of the material is less than the distortion energy per unit volume required to cause yield in a tensile-test specimen. Von Mises stress, also known as Huber stress, is a measure that accounts for all six stress components of a general 3-D state of stress. Von Mises stress σ_{VM}, can be expressed either by six stress components as;

$$\sigma_{MV} = \sqrt{\frac{\left((\sigma_x - \sigma_y)^{\,2} + (\sigma_z - \sigma_x)^{\,2} + (\sigma_y - \sigma_z)^{\,2}\right)}{2} + 3\left(\tau_{xy}^2 + \tau_{xz}^2 + \tau_{yz}^2\right)} \tag{3.65}$$

Von Mises stress σ_{MV}, can be also expressed their principal stresses as:

$$\sigma_{MV} = \sqrt{\frac{1}{2}\left((\sigma_3 - \sigma_1)^{\,2} + (\sigma_1 - \sigma_2)^{\,2} + (\sigma_2 - \sigma_3)^{\,2}\right)} \tag{3.66}$$

The maximum von Mises stress failure criterion is based on the von Mises-Hencky theory, also known as the scalar-energy theory or the maximum distortion energy theory. The theory states that a ductile material starts to yield at a location when the von Mises stress becomes equal to the stress limit. In most cases, the yield strength is used as the stress limit.

Chapter 4

MATERIAL AND METHODOLOGY

Under this chapter 3D model of steam turbine blade with detail, material composition and properties are illustrated. This blade profile and blade material are taken from steam turbine manufacturer Dresser-Rand company catalog. In addition, the basic methodology of ANSYS Work bench setups are explained.

4.1 Three Dimensional Steam Turbine Blade Modelling

Three-dimensional CAD geometric modelling of blade is modelled using Solid Work 2018 software. The blade profile is generated from NACA 2412 blade database (APPENDIX B) copy to Microsoft Excel 2016 to change in to three coordinate and export to Solid Work workbench. This study is only focused on a single blade of steam turbine, which represent multistage turbines.

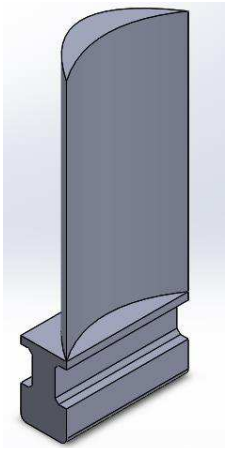

Figure 4.1: Three Dimensional model of steam turbine blade

4.2 Materials of Steam Turbine Blade

Steam turbine blade (STB) is exposed to high pressure and temperature during its operation. The material used for STB must resist this high temperature. The steam turbine blade used in Fincha Sugar Factory is made up of martensitic stainless steel, which is designated by Euronorms as EN-X20Cr13 M.No.1.4029 or AISI 420. Martensitic stainless steels are similar to low alloy or carbon steels, having a structure similar to the ferritics but due to the addition of carbon, it can be hardened and strengthened by heat treatment. Table 4.1 Shows the composition of X20Cr13 stainless steel in percentage. Different stainless steel have different alloys to improve the mechanical and physical properties [52].

Table 4.1: Composition of EN-X20Cr13 M.No.1.4029 stainless steel in percentage (%)

Grade	Iron(Fe)	Chromium(Cr)	Manganese(Mn)	Silicon(Si)	Potassium(P)	Sulphur(S)
420	83.93	14.00	1.00	1.00	0.04	0.03

The effects of the alloying elements

The alloying elements each have a specific effect on the properties of the steel.

Chromium (Cr)

This is the most important alloying element in stainless steels. This element gives the stainless steels their basic corrosion resistance. The corrosion resistance increases with increasing chromium content. It also increases the resistance to oxidation at high temperatures.

Manganese (Mn)

Manganese is generally used in stainless steels in order to improve hot ductility. Its effect on the ferrite/austenite balance varies with temperature: at low temperature, manganese is an austenite stabiliser but at high temperatures, it will stabilise ferrite. Manganese increases the solubility of nitrogen and is used to obtain high nitrogen contents in austenitic steels.

Silicon (Si)

Silicon increases the resistance to oxidation, both at high temperatures and in strongly oxidizing solutions at lower temperatures.

Sulphur (S)

Sulphur is added to certain stainless steels, the free-machining grades, in order to increase the machinability. At the levels present in these grades, Sulphur will substantially reduce corrosion resistance, ductility and fabrication properties, such as weldability and formability. Table 4.2 shows the mechanical properties of EN-X20Cr13 M.No.1.4029 stainless steel take from standard [52].

Table 4.2: Mechanical properties of EN-X20Cr13 M.No.1.4029 (AISI 420)

Properties	Amount
Density	7700 Kg/m^2
Youngs Modulus	192.8 GPa
Yield strength	311 MPa
Poision ratio	0.285
Hardness Brinell	255
Tensile strength	1235 MPa
Endurance limit	669 MPa
Specific heat capacity	535.9 $J/Kg.k$
Coefficient of thermal expansion	12.3x10-6
Thermal conductivity	25.3 W/mk

4.3 Setup in ANSYS Workbench

ANSYS Workbench 19.0 has a module for FSI analysis. In FSI analysis method, data mapping of edges and meshing of the geometries are very interesting point. To consider this ANSYS CFX is selected for this study area than ANSYS FLUENT.Because ANSYS CFX uses a vertex-centered approach and sticks to just the traditional tetrahedral and hexahedral mesh topology. However, ANSYS FLUENT uses a cell-centered approach, polyhedral mesh and cut cell meshes. In this module the fluid flow analysis is using CFX and static structure analysis for solid mechanics. As figure 4.4 shown below the geometry is linked with both CFX and static structure module from geometry module. The solution calculated from fluid flow is linked to the setup of the structure to transfer fluid load. Since there is no steam option fluid in the CFX setup create the new fluid material using the properties of steam.

4.3.1 Element type for Finite Element Analysis (FEA)

Elements fall into four major categories: 2D line elements, 2D planar elements, and 3D solid elements which are all used to define geometry; and special elements used to apply boundary conditions. Special elements might include gap elements to specify a gap between two pieces of geometry. Generally, there are two main methods of grid generation in Finite Element Analysis (FEA): structured grid (Cartesian and curvilinear) and unstructured grid (tetrahedral and quadrilateral). Unstructured grid generation approach is used for both fluid and structure meshing. The reason is:

- The grid density can be controlled in any region without worrying much about the density getting increased in another region.

- Easy to use with complex geometries. Can be computed within an hour.
- Do not have to worry much about skewness or bad quality since the grid generation algorithm takes care of that most of the time.

Tetrahedral meshing is appropriate for uses in viscous flow simulations are wished-for.

4.4 Mesh for fluid analysis

The mesh statistics of boundary box is illustrated in figure 4.2 the number of nodes and elements are 1,518,450 and 8,766,605 respectively. The boundary box size are x =190 mm, y = 570 mm, and z = 450 mm. This meshing is very important in ANSYS simulation because the result is differ when the number of nodes and elements are changed.

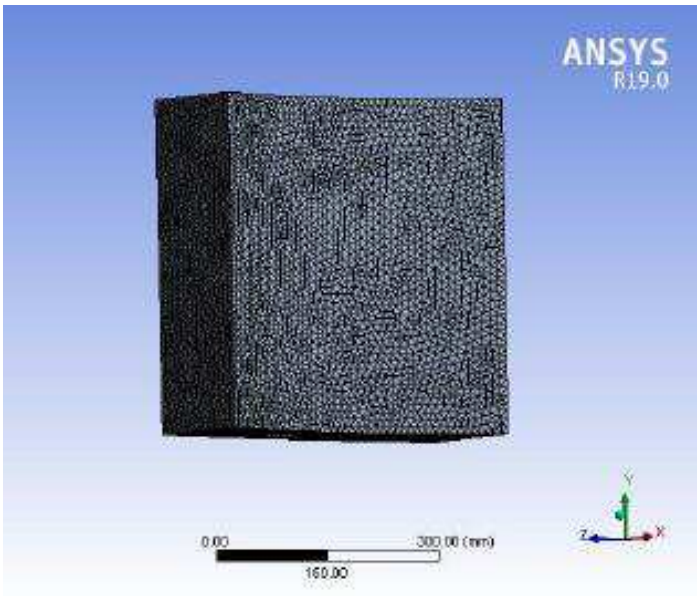

Figure 4.2: Mesh statistics of boundary box

Figure 4.3 illustrate that the graphical representation of mesh statistics (number of nodes and elements) verses element size of boundary box. As the size of element in meshing increases both the number of nodes and elements are decrease.

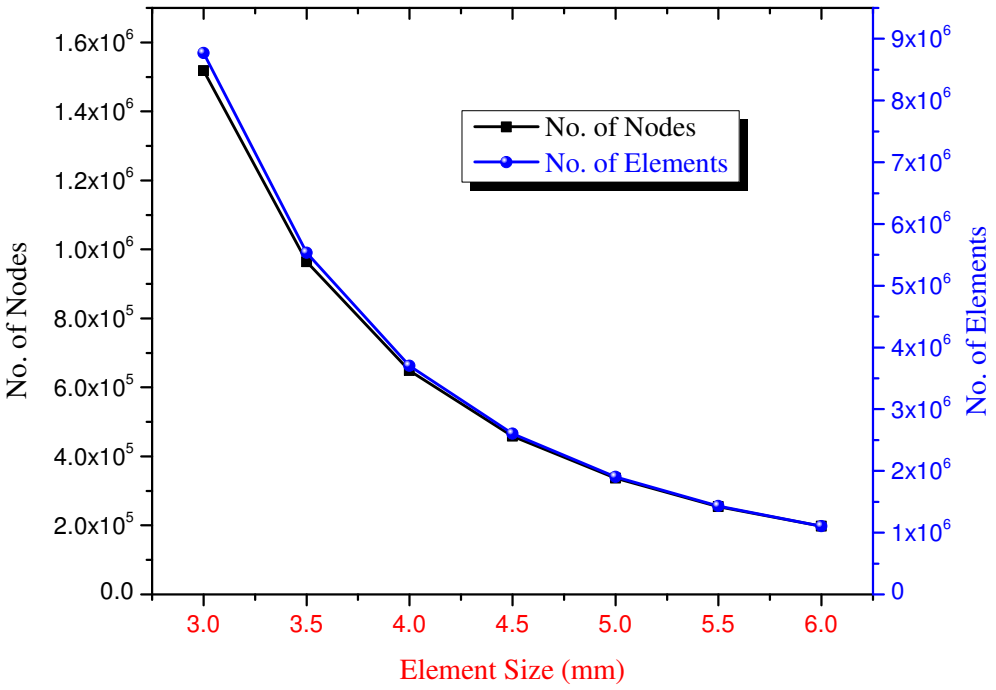

Figure 4.3: Mesh statistics of boundary box verses element size

4.5 Mesh for structural analysis

In figure 4.4 the number of nodes and elements are 1,583,574 and 1,133,210 respectively. The meshing or gridding type used for this analysis is unstructured grid method. Under this method, divide 3D model of the blade in to finite number of elements, which is called tetrahedrons. After discretization blade by meshing then applying boundary condition in order to get the simulation result.

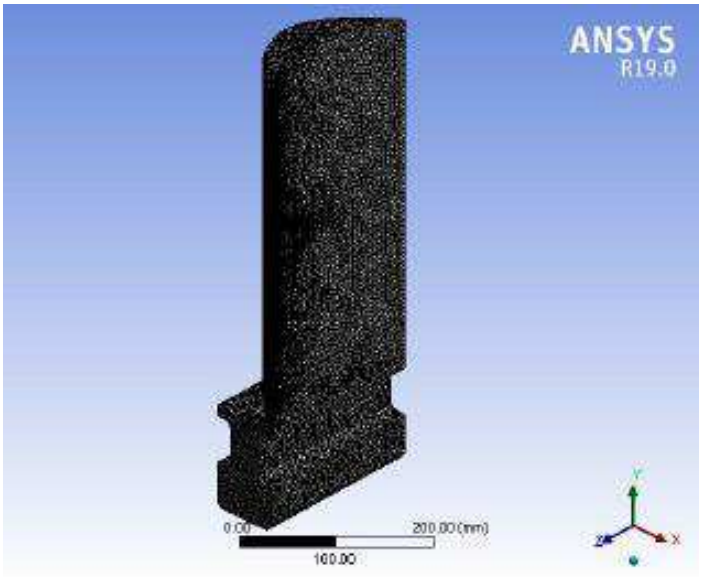

Figure 4.4: Mesh statistics of steam turbine blade

Figure 4.5 illustrate that the graphical representation of mesh statistics (number of nodes and elements) verses element size of steam turbine blade. As the size of element in meshing increases both the number of nodes and elements are decrease.

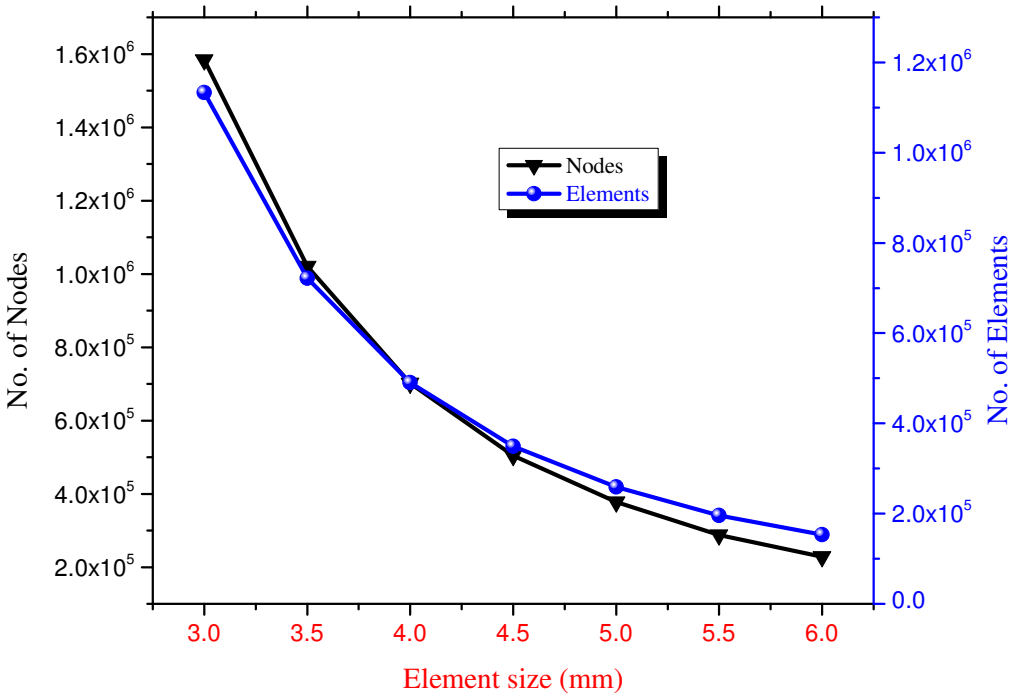

Figure 4.5: Mesh statistics of steam turbine blade verses element size

In general, mesh statistics of both fluid and solid are summarized as table 4.3.In this table the number of nodes and elements generated based on the element size of 3mm.

Table 4.3: Mesh Statistics FSI

Mesh statistics	Fluid	Solid	Total
Number of nodes	1,518,450	1,583,574	3,102,024
Number of elements	8,766,605	1,133,210	9,899,815
Element size(mm)	3	3	

4.6 FSI Coupling

As explained in section 3.1 FSI method of analysis is divided in to two namely monolithic (fully coupled) and partitioned (staggered) approach. This study only consider the effect of fluid on the solid but not vice versa. This way of analysis approach is known as one way FSI coupling. The following steps are considered to analyze fatigue life.

For fluid flow (CFX) the steps followed is as below:

1. Importing 3D geometry into ANSYS 19.0 workbench in block A2 and automatically the geometry imported is activated in both block B2 and block C3.
2. Generating tetrahedral topology mesh is generated for fluid flow (CFX) in block B3 as shown in figure 4.2.
3. In block B4 the basic setup considered are transient analysis type in time step, create boundary domain and boundary condition; create new fluid material using steam properties, select LES Smagorinsky turbulence model, setting solver control and output control.
4. To start the simulation in block B5 select double precision and Intel MPI Local Parallel run mode then click start run.
5. At the last, check the results in block B6.

For static structure steps:

1. Set the engineering data for steam turbine blade EN-X20Cr13 using its properties in block C2.
2. Check whether geometry is imported or not in block C3.
3. In (Model) block C4 setting mesh in 3mm body size as shown in figure 4.4, setting the boundary condition by applying fixed support, apply tangential, axial and body force on the blade.
4. Check the output solution of fluid flow analysis (block B5) is connected with the setup of static structure (block C5) to import pressure and temperature loads.
5. Inserting total deformation, equivalent (Von Mises) stress, maximum and minimum principal stress in solution (block C6).
6. In addition, inserting fatigue tool in block C6 and consider fully reversed loading type, stress-life analyses type and Goodman mean stress theory.
7. At the end, discuss the result in block C7.

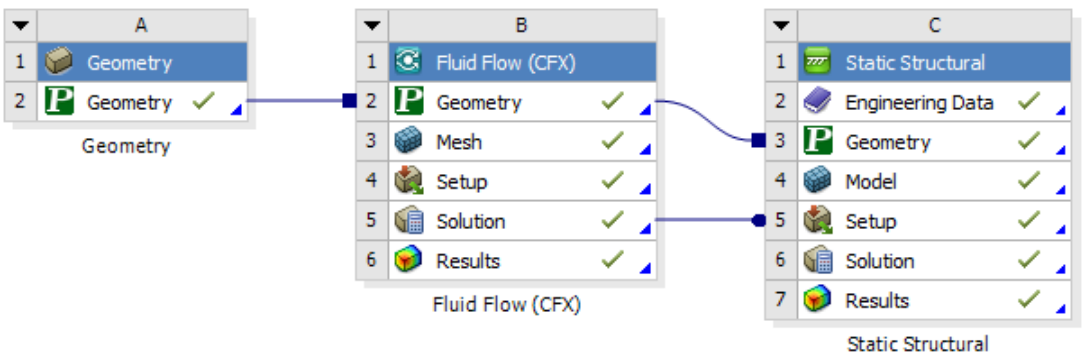

Figure 4.6: ANSYS Workbench FSI tool

Chapter 5

RESULT AND DISCUSSION

5.1 Computational Fluid Dynamics Analysis Result

In this study, the CFD analysis is aimed to investigate the pressure distribution on the turbine blade. In FSI module fluid flow, ANSYS CFX is linked with static structure. The analysis is conducted on the blade length of 0.2 m that is exposed to the inlet boundary condition listed in table 4.3 . The 3-D model blade was imported into a computational fluid domain as shown in figure 4.6. The size of the computational domain is enclosed to rectangular box size is x =190 mm, y = 570 mm, and z = 450 mm. The meshing of fluid domain is demonstrated in figure 4.2. Figure 5.1 demonstrate the pressure distribution on the blade with streamline. Pressure distribution is one parameter analyzed in CFD. The maximum pressure is happened on the front side of the blade at which steam is applied but in other side very low because the blade is impulse type.

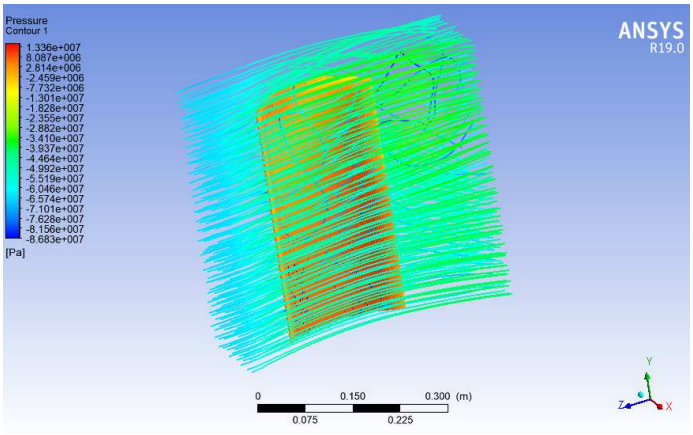

Figure 5.1: Pressure distribution with streamline on the blade

Figure 5.2 shows temperature distribution on the steam turbine blade. Since the temperature of steam is very high, the blade is caused a thermal fatigue. The action of temperature forms a

strain as formulated in equation 3.52.

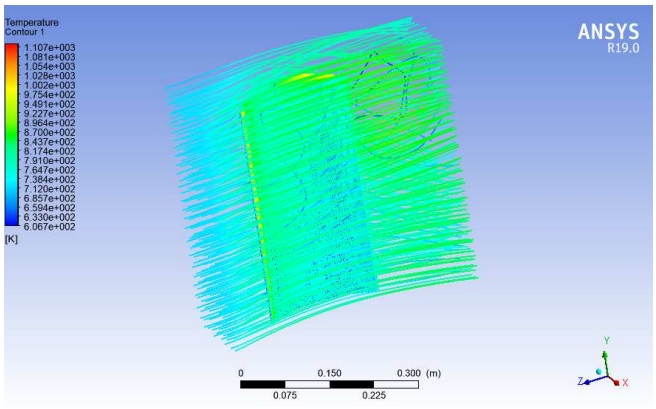

Figure 5.2: Temperature distribution with streamline on the blade

Generally, in CFD simulation the effect of pressure and temperature distribution result is analyzed. This simulation result used to achieve one of the specific objective.

5.2 Static Structural Analysis Result

As figure 4.4 shows the meshing of steam turbine blade that is very important in ANSYS simulation for more approximate result. Figure 5.3 shows the total deformation contour along the blade due to applied loads considered in this study. The total loads applied give result of the maximum total deformation 5.1755 mm, which found at the tip of the blade. As the length of blade increase, the total deformation is also increased as shown.

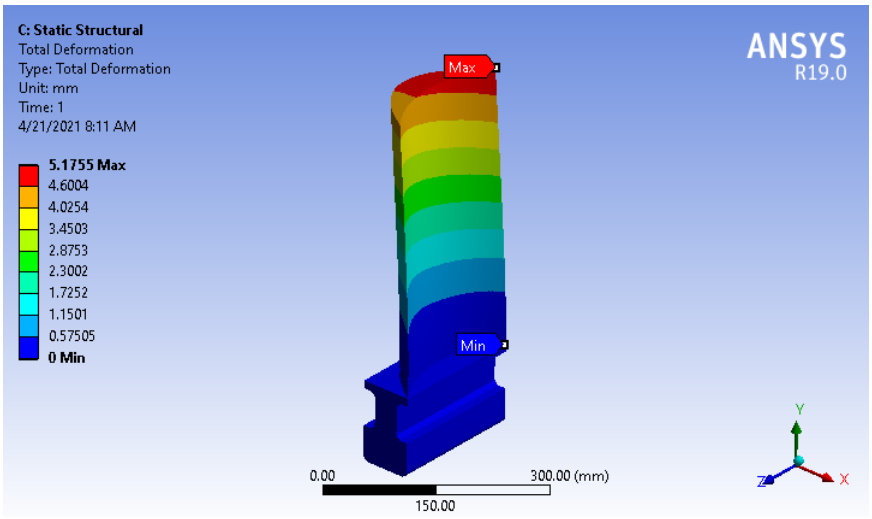

Figure 5.3: Total deformation of steam turbine blade

Figure 5.4 shows the equivalent (von-Mises) stress distribution contour and the maximum Von-Mises stress is 1983.8 MPa and the minimum Von-Mises stress is 0 MPa. From this simulation

stress analysis of the blade, maximum stress is generated around the root of the blade.

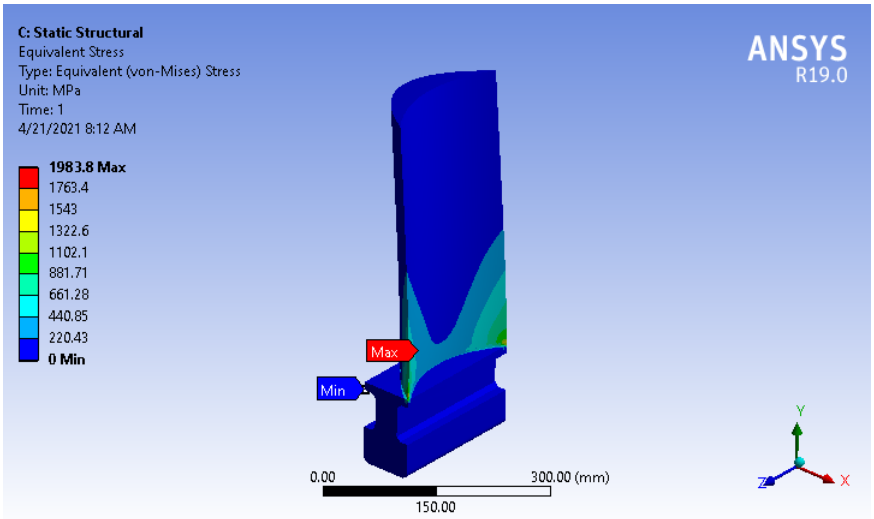

Figure 5.4: Equivalent (Von-Mises) stress of steam turbine blade

Figure 5.5 demonstrate that the maximum principal stress is 1453.2 MPa. The simulation of this stress analysis result on the blade show that maximum stress generated is found at the site similar to equivalent stress as shown in figure 5.4 around the root of the blade.

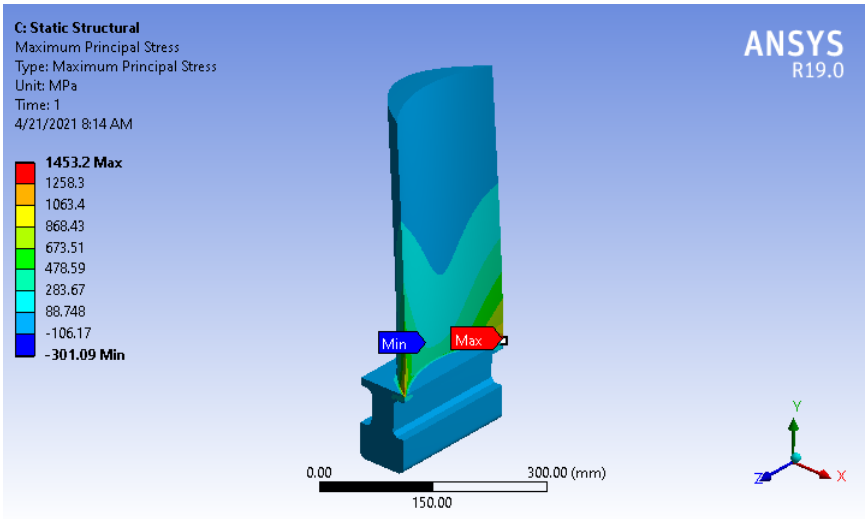

Figure 5.5: Maximum principal stress of steam turbine blade

Figure 5.6 shows the minimum principal stress of the blade with the maximum value of 296.52 MPa and minimum value of -2051 MPa. The negative sign shows stress are totally under compression.

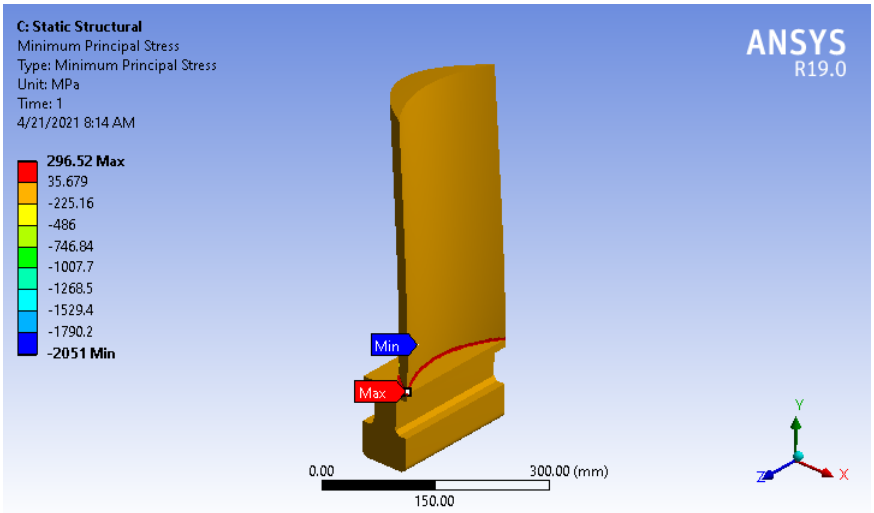

Figure 5.6: Minimum principal stress of steam turbine blade

5.3 Life Analysis of the Steam Turbine Blade

From ANSYS analysis result figure 5.7 fatigue life of steam turbine blade is approximated. Steam turbine used in Fincha Sugar Factory is operated for nine months because the left three months the factory is under overall annual maintenance and summer season there is no sugar cane feeding to factory. The fatigue life of the geometry model is found to be 4.5067e10 cycles. Therefore the three dimensional engineering model of a steam turbine blade can operate for minimum of 19.42 years, which means that a machine operating at 5970 rpm will be exposed to Year x 270 x 24 x 60 x 5970 rpm = 4.5067e10 stress cycles.

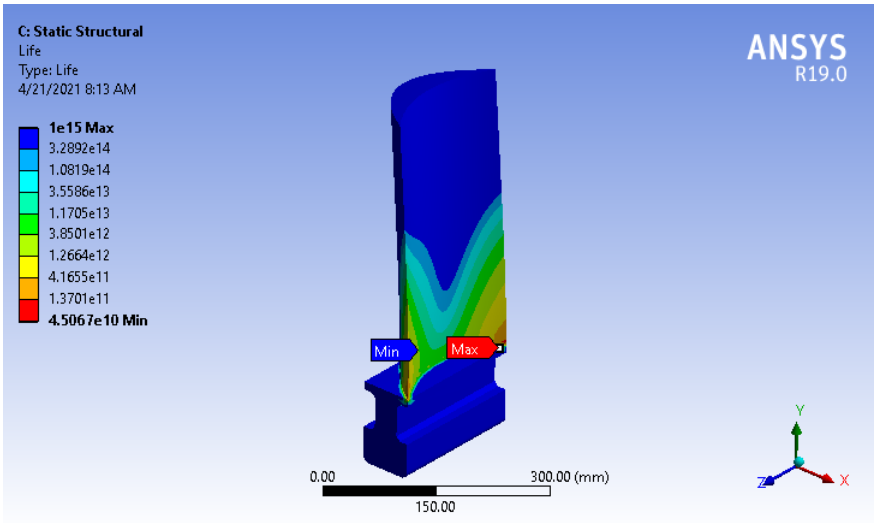

Figure 5.7: Fatigue life of steam turbine blade

Figure 5.8 shows that the safety factor of the blade is 2.0158 approximately two, which implies the steam turbine blade, will account for twice of the expected forces. Therefore, the steam

turbine blade is safe for the applied loads.

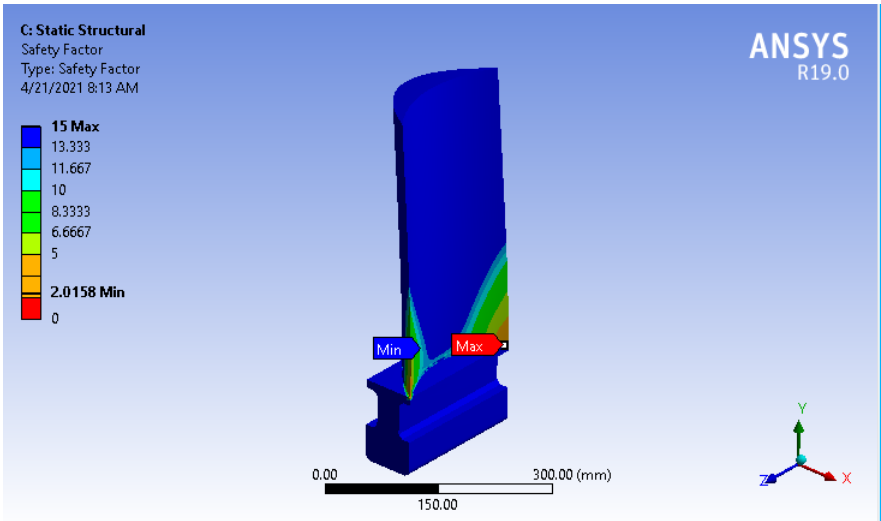

Figure 5.8: Safety factor of the blade

In general, the static structural analysis result is summarized as table 5.1. The result tabulated in table 5.1 is at the element size of 3 mm for both fluid and solid.

Table 5.1: The static structural analysis result

S.No	Static Structural Analysis	Maximum value	Minimum value
1	Total deformation (mm)	5.1755	0
2	Equivalent (Von-Mises) stress (MPa)	1983.8	0
3	Maximum principal stress (MPa)	1453.2	-301.09
4	Minimum principal stress (MPa)	296.52	-2051
5	Fatigue life (cycle)	1e15	4.5067e10
6	Safety factor	15	2.0158

Figure 5.9 shows the comparative of element size verses static structure analysis result (total deformation, maximum Von-Mises stress and maximum principal stress). The variation of element size is from 3 mm to 6 mm in 0.5 mm increments. In this, the element size variation is only for structure but the element size for fluid is keeping 3 mm.

As shown in figure 5.9, as the element size increase the value of all total deformation, maximum Von-Mises stress and maximum principal stress are decrease.

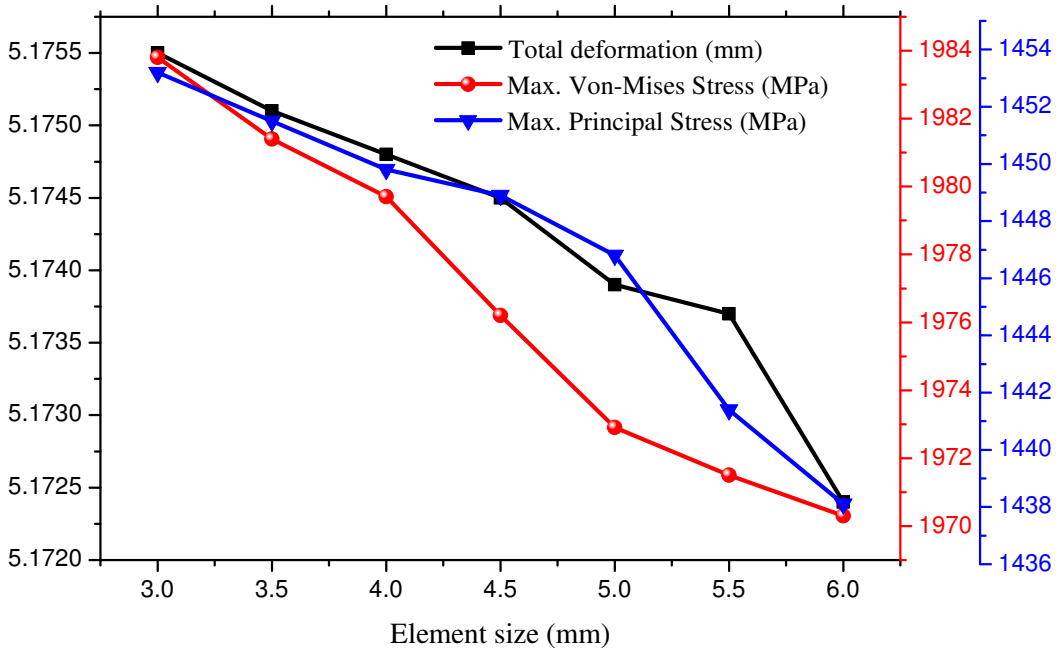

Figure 5.9: Element size verses static structure analysis result

5.4 Stress amplitude - Number of cycle to failure (S-N) curve or fatigue curve

A S-N Curve is a plot of the magnitude of an alternating stress versus the number of cycles to failure for a given material. Typically, both the stress and number of cycles are displayed on logarithmic scales. Using Basquin relation as illustrated in equation 3.62 the log-log scale of fatigue curve is drawn as figure 5.11. S-N curve shows the endurance limit at which failure occurs as number of cycle becomes very large. At this endurance or fatigue limit the stress amplitude is called as fatigue strength. At zero number of cycle the stress amplitude reaches ultimate stress a point at which failure occurred. Fatigue analysis was carried out for the blade in the ANSYS workbench module using mean stress theory as shown in figure 5.10. The material data consisting of S-N curves for the given components were obtained from various sources and inserted into the software's engineering material database. A fully reversed figure 5.10(a)and Goodman method figure 5.10(b) of mean stress was used for the loading cycle.

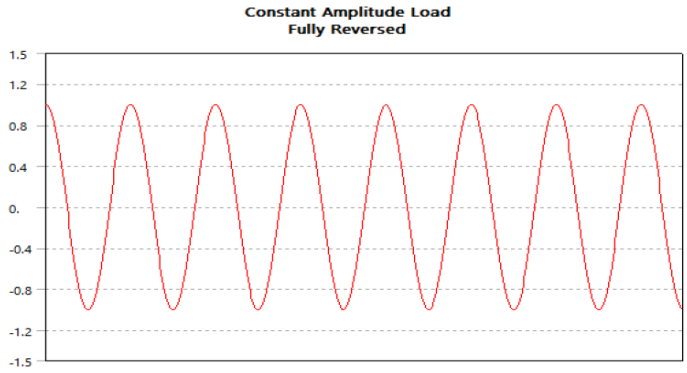

(a)

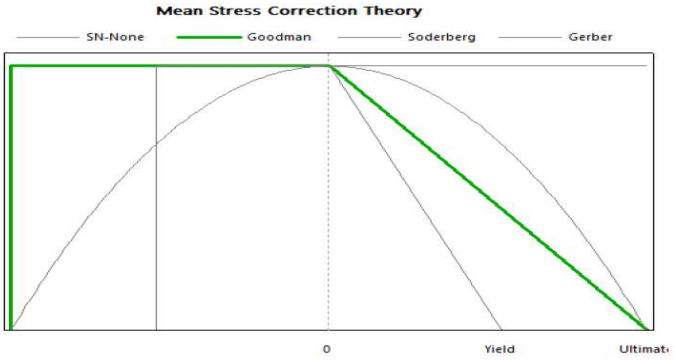

(b)

Figure 5.10: Fully reversed load cycle and Goodman diagram

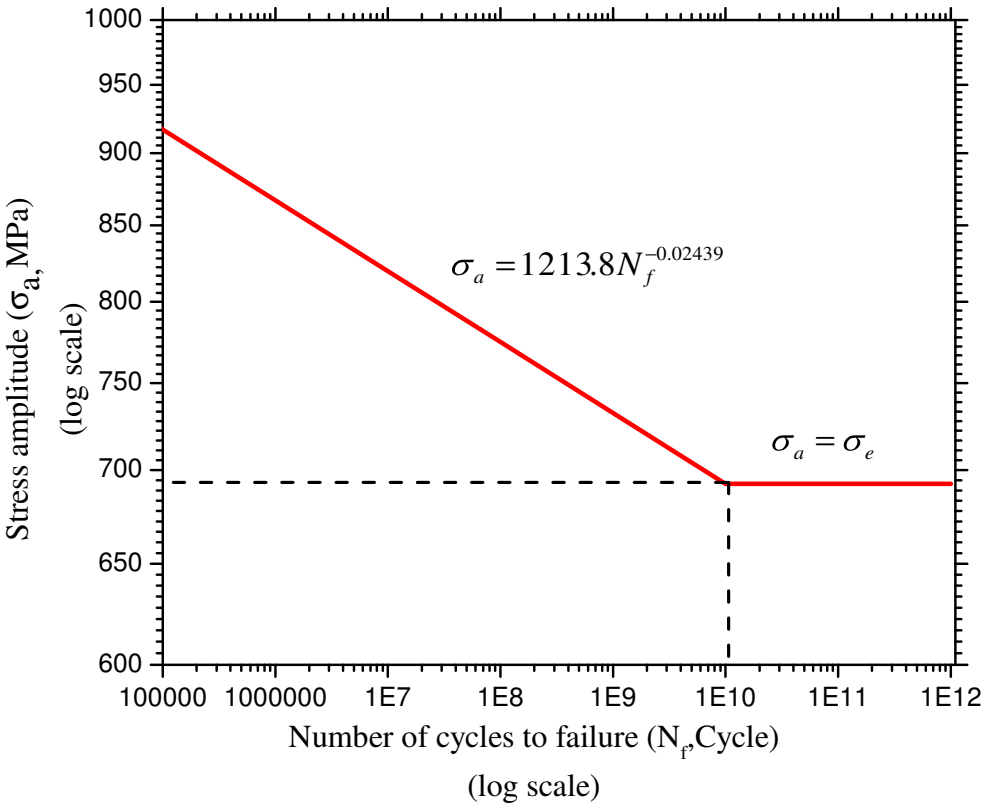

Figure 5.11: Stress amplitude versus number of cycle to failure (S-N) curve

Chapter 6

CONCLUSIONS AND RECOMMENDATIONS

6.1 Conclusion

The fatigue failure of steam turbine blade is the failure without contact of other body. The FSI method of analysis is used for this study, which is analyzing the effect of steam on the blade structure. This case study focus on impulse steam turbine blade operates in Finchaa Sugar Factory and technical data of steam turbine is illustrate in table 3.1. In this study, both FVM for CFD and FEM for static structure are formulated mathematically by considering a transient state because fatigue failure is happened due to cyclic load. The loads value was calculated to carry out a stress analysis of the blade model and thus regions of high stress concentration were observed from the ANSYS analysis results in both CFD and static structural. A stress based approach for fatigue analysis was preferred than a strain based one because the steam turbine blade operate under high cyclic. In CFD analysis pressure and temperature distribution is implemented as output result. In this CFD study, the working fluid is steam, which is not available as option in ANSYS CFX so creating as material using its basic properties. In addition, in static structural analysis the maximum total deformation is 5.1755 mm and the minimum total deformation is zero, maximum equivalent Von Mises stress is 1983.8 MPa and minimum equivalent Von Mises stress is zero, and the maximum principal stress 1453.2 MPa is determined. Finally, fatigue life prediction analysis was implemented on the blade model by referring from fatigue tools in ANSYS 19.0 and results 4.5067e10 cycles.

In order to achieve the goal of this study, a lot of work was performed and the following conclusions are drawn.

- Mathematical modeling for both fluid dynamics and solid dynamics are formulated in transient state.
- The highly stress concentration location of steam turbine blade is at the hub.
- The fatigue life of the blade is 19.42 years..

6.2 Recommendation

Many researchers conducted study on steam turbine blade design in the world for different type of steam turbine. In Finchaa Sugar Factory, impulse type steam turbine is operating for a last twenty-one years ago it needs more attention and conducting research on it as some area of study listed in future work. In order to withstand fatigue failure, the recent steam turbine blade technology is recommended. Because the composition of steel alloy affects the life of blade. Therefore, annual steam turbine maintenance is essential to check the failure part of blade.

Future Work

The following aspects should be considered for further work on this thesis:

- Monolithic (Fully coupled) FSI approach may used for mathematical modeling and COMSOL software.
- The analysis by assessing other cause of failure of the blade, such as vibration, impact analysis, corrosion effect, erosion effect and others.
- Repeat the analysis using other methods like conjugate heat transfer.
- Identify and improve the life of crack initiation and propagation.
- The work could be done by considering the effect of startup and shutdown of the steam turbine.
- The work could be done by considering the effect of steam quality on the life of the blade.

Bibliography

[1] Dulau M and Bica D. Simulation of speed steam turbine control system. *Procedia Technology*, 12:716–722, 2014.

[2] Solanki RS Gupta GK Saxena S, Pandey JP and Modi OP. Coupled mechanical, metallurgical and fem based failure investigation of steam turbine blade. *Engineering Failure Analysis*, 52:35–44, 2015.

[3] Jachens WB. Steam turbine- their construction, selection and operation. proceedings of the south african sugar technologies association.

[4] Leela Krishna V. High pressure impulse steam turbine blade. 2013.

[5] Prabhunandan GS and Byregowda HV. Static and fatigue analysis of a steam turbine blade. *International Journal of Latest Technology in Engineering, Management and Applied Science*, 2016.

[6] Srivastava KP and Pancholi NH. A review on analysis of low pressure stage of steam turbine blade with fea (ansys software).

[7] Gupta P Bhagi LK and Rastogi V. Fractographic investigations of the failure of l-1 low pressure steam turbine blade. *case studies in Engineering Failure Analysis*, 1(2):72–78, 2013.

[8] Martinelli L Jameson A and Pierce NA. Optimum aerodynamic design using the navier–stokes equations. *Theoretical and computational fluid dynamics*, 10(1):213–237, 1998.

[9] Sayma and Abdulnaser. *Computational fluid dynamics*. Bookboon, 2009.

[10] Shukla AK Prasad YM and Roy A. Analysis of transient thermal cycling for life assessment of steam turbine rotors. 2007.

[11] Sen PK Patel TK and Sharma R. Review on common failure of steam turbine blade. *International Journal of Research (IJR)*, 2(11):137–141, 2015.

[12] `http://en.Wikipedia.Org/w/index.Php?Oldid=410183540`.

[13] https://folk.ntnu.no/haugwarb/TKP4175/History/historyofsteampower.pdf.

[14] https://en.Wikipedia.Org/wiki/history_of_the_steam_engine.

[15] https://en.Wikipedia.Org/wiki/steam_turbine.

[16] Bergallo B Ziegler D, Puccinelli M and A. Picasso. Investigation of turbine blade failure in a thermal power plant. *Case Studies in Engineering Failure Analysis*, 1(3):192–199, 2013.

[17] Ray AK Das SK Das G, Chowdhury SG and Bhattacharya DK. Turbine blade failure in a thermal power plant. *Engineering failure analysis*, 10(1):85–91, 2003.

[18] Enzinger N Plesiutschnig E, Fritzl P and Sommitsch C. Fracture analysis of a low pressure steam turbine blade. *Case Studies in Engineering Failure Analysis*, 5:39–50, 2016.

[19] M. Nurbanasari. Crack of a first stage blade in a steam turbine. *Case Studies in Engineering Failure Analysis*, 2(2):54–60, 2014.

[20] Garca JC Sz JK, Segura JA and Rodriguez JA. Failure analysis of the 350 mw steam turbine blade root. *Engineering Failure Analysis*, 16(4):1270–1281, 2009.

[21] Azevedo CR and Sintora A. Erosion-fatigue of steam turbine blades. *Engineering Failure Analysis*, 16(7):2290–2303, 2009.

[22] Shlyannikov M Citarella R, Lepore M and R. Yarullin. Fatigue crack growth by femdbem approach in a steam turbine blade. *Industrial Engineering and Management*, 4(160):2169–2173, 2015.

[23] M. Banaszkiewicz. The low-cycle fatigue life assessment method for online monitoring of steam turbine rotors. *International Journal of Fatigue*, 113:311–323, 2018.

[24] Suhas B and Khan A. Fatigue and creep interaction in steamturbine bladed disk. *International Journal of Innovative Research in Science, Engineering and Technology*, 3, 2014.

[25] Shantharaja M Tulsidas D and Bharath VG. Life estimation of a steam turbine blade using low cycle fatigue analysis. *Procedia Materials Science*, 5:2392–2401, 2014.

[26] Rosales I Rodriguez JA Urquiza G Segura JA, Castro L and Rodriguez JM. Diagnostic and failure analysis in blades of a 300 mw steam turbine. *Engineering Failure Analysis*, 82:631–641, 2017.

[27] Jk. Sz. Failure analysis of steam turbine last stage blade tenon and shroud. *Engineering Failure Analysis*, 14(8):1476–1487, 2007.

[28] Majid Y Nikravesh and MeidanSharafi M. Failure of a steam turbine rotor due to circumferential crack growth influenced by temperature and steady torsion. *Engineering Failure*

Analysis, 66:296–311, 2016.

[29] Askhedkar RD Ghugal, Sandip G and Choudhary SK. Estimation of stress concentration factor and strain concentration factor in steam turbine blade by finite element method. 2013.

[30] Chebrolu K Ramana AR Bhargav R, Student MT and Raju TD. Structural and thermal analysis of steam turbine blade using fem.

[31] Klenk A Wang WZ, Buhl P and Liu YZ. The effect of in-service steam temperature transients on the damage behavior of a steam turbine rotor. *International Journal of Fatigue*, 87:471–483, 2016.

[32] Stein P Fadl M and He L. Full conjugate heat transfer modelling for steam turbines in transient operations. *International Journal of Thermal Sciences*, 124:240–250, 2018.

[33] Klenk A Wang WZ, Buhl P and YZ. Liu. Study of creep–fatigue behavior in a 1000 mw rotor using a unified viscoplastic constitutive model with damage. *International Journal of Damage Mechanics*, 25(2):178–202, 2016.

[34] Nowakowska A Pawlicki J Borkowski P, Gowacki D and Zwoliski J. Fe analysis of a steam turbine hp rotor blade stage concerning material effort, dynamic properties and creep damage assessment. *Archive of Mechanical Engineering*, 63(1):163–185, 2016.

[35] Mangani L Moukalled F and Darwish M. *The finite volume method in computational fluid dynamics*, volume 6. Springer, 2016.

[36] Versteeg HK and Malalasekera W. *An introduction to computational fluid dynamics: the finite volume method*. Pearson education, 2007.

[37] Dalisay and Jon D. Mechanics of fluids.

[38] Kolmogorov AN. Equations of turbulent motion in an incompressible fluid. In *Dokl. Akad. Nauk SSSR*, volume 30, pages 299–303, 1941.

[39] Jones WP and Launder BE. The prediction of laminarization with a two-equation model of turbulence. *International journal of heat and mass transfer*, 15(2):301–314, 1972.

[40] Launder BE and Sharma BI. Application of the energy-dissipation model of turbulence to the calculation of flow near a spinning disc. *Letters in heat and mass transfer*, 1(2):131–137, 1974.

[41] Leonard A. Large-eddy simulation of chaotic convection and beyond. In *35th Aerospace Sciences Meeting and Exhibit*, page 204, 1997.

[42] Schmitt FG. About boussinesq's turbulent viscosity hypothesis: historical remarks and a direct evaluation of its validity. *Comptes Rendus Mécanique*, 335(9-10):617–627, 2007.

[43] Smagorinsky J. General circulation experiments with the primitive equations: I. the basic experiment. *Monthly weather review*, 91(3):99–164, 1963.

[44] Peric M Street Ferziger, Joel H and Robert L. *Computational methods for fluid dynamics*, volume 3. Springer, 2002.

[45] Schmidt W Jameson A and Turkel E. Numerical solution of the euler equations by finite volume methods using runge kutta time stepping schemes. In *14th fluid and plasma dynamics conference*, page 1259, 1981.

[46] Liu F and Zheng X. A strongly coupled time-marching method for solving the navier-stokes and kw turbulence model equations with multigrid. *Journal of Computational Physics*, 128(2):289–300, 1996.

[47] Bader Q and Kadum E. Mean stress correction effects on the fatigue life behavior of steel alloys by using stress life approach theories. *International Journal of Engineering & Technology IJETIJENS*, 10:p50, 2014.

[48] Kim HS. *Mechanics of solids and fracture*. bookboon. com, 2017.

[49] Andrade Jr Jose S Kun F, Carmona HA and Herrmann HJ. Universality behind basquins law of fatigue. *Physical review letters*, 100(9):094301, 2008.

[50] RS Khurmi and JK Gupta. *A textbook of machine design*. Eurasia, 2005.

[51] Richard G Budynas, J Keith Nisbett, and Kiatfa Tangchaichit. *Shigley's mechanical engineering design*. McGraw Hill New York, 2005.

[52] Atlas Steels. Stainless steel grade datasheets. *Atlas Steels Technical Department*, 2013.

APPENDIX

APPENDIX A: Image Taken From Ficha Sugar Factory

A. Steam Turbine Specification

B. First Unit Steam Turbine

C. Inlet Direction of Steam into Turbine

D. Steam Turbine Connected With Generator.

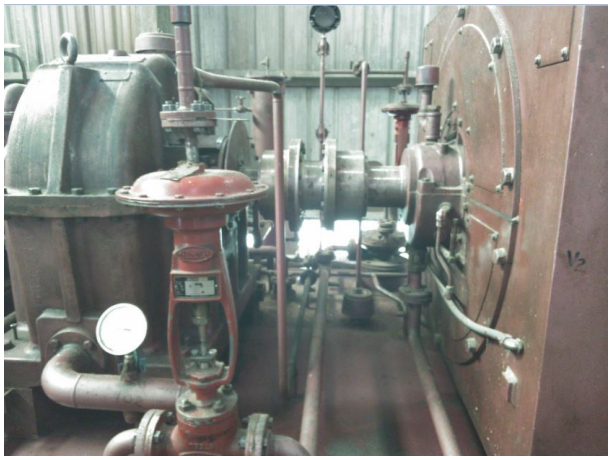

APPENDIX B: NACA2414 Database and airofoil shape

X	Y	X	Y
1.000084	0.001257	0.000000	0.000000
0.998557	0.001575	0.002223	-0.006689
0.993984	0.002524	0.007479	-0.012828

0.986392	0.004086	0.015723	-0.018404
0.975825	0.006231	0.026892	-0.023408
0.962343	0.008922	0.040906	-0.027826
0.946027	0.01211	0.057669	-0.031651
0.926971	0.01574	0.077071	-0.034878
0.905287	0.019752	0.098987	-0.037507
0.881104	0.024079	0.123281	-0.039546
0.854565	0.028653	0.149805	-0.041013
0.82583	0.033404	0.178401	-0.041934
0.795069	0.03826	0.208902	-0.042346
0.762469	0.043149	0.241131	-0.042294
0.728228	0.048	0.274904	-0.041834
0.692554	0.052741	0.310028	-0.041027
0.655665	0.057302	0.346303	-0.039941
0.617788	0.061615	0.383522	-0.038644
0.579155	0.065609	0.421644	-0.037174
0.540008	0.06922	0.460397	-0.035444
0.500588	0.072381	0.499412	-0.033493
0.461143	0.075034	0.538451	-0.031373
0.421921	0.077122	0.577279	-0.029138
0.383032	0.078574	0.615658	-0.026833
0.34468	0.079198	0.653352	-0.0245
0.307289	0.078941	0.690129	-0.022172
0.271106	0.077802	0.725762	-0.01988
0.236371	0.075794	0.760029	-0.017649
0.203313	0.072947	0.792716	-0.015499
0.172151	0.069309	0.823619	-0.013448
0.143088	0.064941	0.852541	-0.01151
0.116313	0.059918	0.879302	-0.009701
0.091996	0.054325	0.90373	-0.008033
0.070289	0.048257	0.925669	-0.00652
0.051324	0.041808	0.944979	-0.005174

0.035214	0.035076	0.961536	-0.004008
0.022051	0.028152	0.975232	-0.003035
0.011907	0.02112	0.985978	-0.002265
0.004833	0.014049	0.993705	-0.001708
0.00086	0.006997	0.998361	-0.00137
		0.999916	-0.001257

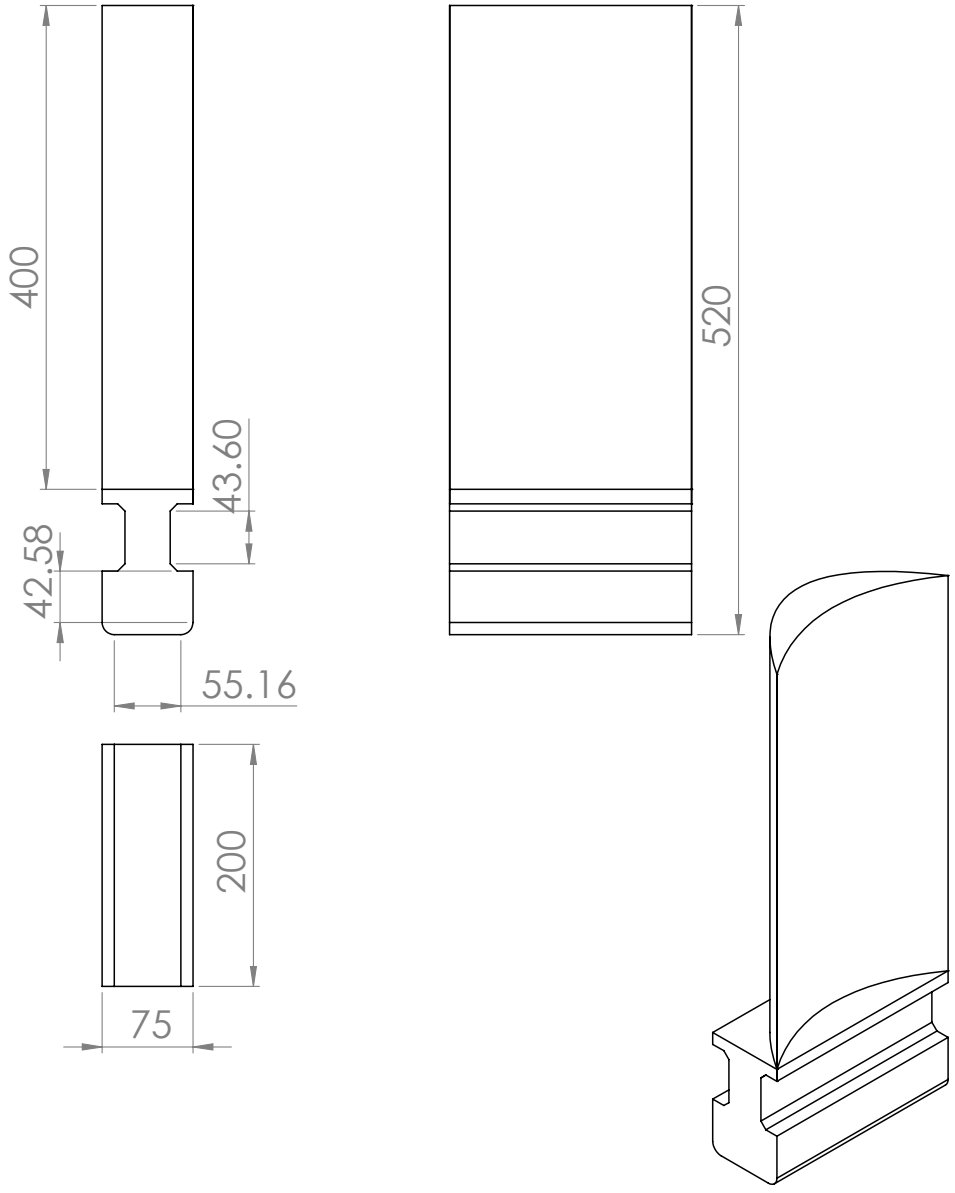

UNLESS OTHERWISE SPECIFIED: DIMENSIONS ARE IN MILLIMETERS SURFACE FINISH: TOLERANCES: LINEAR: ANGULAR:		FINISH:			DEBUR AND BREAK SHARP EDGES	DO NOT SCALE DRAWING	REVISION
	NAME	SIGNATURE	DATE			TITLE:STEAM TURBINE BLADE	
DRAWN	MOTI T						
CHK'D							
APPV'D							
MFG							
Q.A				MATERIAL: AISI 420		DWG NO. 1	A4
				WEIGHT:		SCALE:1:1	SHEET 1 OF 1